IEEE Access
Multidisciplinary | Rapid Review | Open Access Journal

Received 18 September 2023, accepted 12 October 2023, date of publication 23 October 2023, date of current version 27 October 2023.

Digital Object Identifier 10.1109/ACCESS.2023.3326443

SURVEY

THz Communications: A Key Enabler for Future Cellular Networks

NAJAM US SAQIB[2], (Graduate Student Member, IEEE), MUHAMMAD SAJID HAROON[2], HWI YOUNG LEE[3,4], KWANGHYUN PARK[3], HOON-GEUN SONG[3], AND SANG-WOON JEON[1,2], (Senior Member, IEEE)

[1]School of Computer Science and Technology, Zhejiang Normal University, Jinhua 321004, China
[2]Department of Electrical and Electronic Engineering, Hanyang University, Ansan 15588, South Korea
[3]Future Communication Technology Center, Korea Testing Laboratory, Ansan 15588, South Korea
[4]Department of Electrical and Computer Engineering, Sungkyunkwan University, Suwon 16419, South Korea

Corresponding author: Sang-Woon Jeon (sangwoonjeon@hanyang.ac.kr)

This work was supported by Institute of Information & Communications Technology Planning & Evaluation (IITP) grant funded by the Korea government (MSIT) (No. 2022-0-00868, Development of high resolution vector network analyzer HW platform supporting Sub-THz frequency band).

ABSTRACT Future cellular networks are expected to benefit from terahertz (THz) frequency bands, which enable high-speed and low-latency wireless connectivity, but several challenges have arisen in utilizing THz bands. In this paper, we first investigate channel characteristics and their modeling for THz bands, highlighting new opportunities and emerging challenges. In this context, we discuss the channel characteristics that become more prominent at THz frequencies than at lower microwave frequencies, such as atmospheric attenuation, scattering, and frequency selectivity. We also review various path-loss and scattering models for THz communications. We further survey the radio frequency front-end nonlinearities that affect THz communications and their modeling for multiple-input multiple-output (MIMO) systems. We then review massive MIMO and hybrid beamforming techniques, and their applicability for THz communications. We identify the challenges that arise from operating at ultra-high frequencies, such as beam blockage, power consumption of large-scale arrays, and beam squint. Finally, we provide an overview of emerging intelligent reflecting surface (IRS) technologies and their potential for enhancing THz wireless networks. We investigate how IRS and massive MIMO technologies can be integrated into THz wireless networks and discuss possible solutions to overcome the limitations that affect the throughput and efficiency of such systems.

INDEX TERMS THz communications, channel modeling, 6G systems, RF front-end nonlinearities, multiple-input and multiple-output (MIMO) techniques, intelligent reflecting surface (IRS).

I. INTRODUCTION

Over the past few years, there has been an enormous growth in wireless data transmission, with the average mobile data rate expected to increase threefold from 2018 to 2023 [1], [2]. This tremendous growth in data rate is mainly driven by the increasing use of mobile devices and the emergence of new technologies and applications that demand high data rates and low latencies. Furthermore, a significant surge in global fourth-generation (4G) and fifth-generation (5G) mobile data traffic is expected, reaching approximately 280 to 290 exabytes per month by 2027, as depicted in Fig. 1 [3], [4]. Additionally, the ITU-R report in [5] estimates that overall global data traffic will approach 5016 exabytes per month by 2030. This surge in data traffic is primarily attributed to the proliferation of smart devices and the deployment of new technologies that facilitate the collection and transmission of vast amounts of data.

The associate editor coordinating the review of this manuscript and approving it for publication was Bilal Khawaja.

TABLE 1. KPIs for 4G, 5G, and 6G [14], [17].

Characteristics	4G	5G	6G
DL data rate	1 Gbps	20 Gbps	1 Tbps
Latency	100 ms	10 ms	Less than 1 ms
Max. spectral efficiency	15 bps/Hz	30 bps/Hz	100 bps/Hz
Operating frequency	2-8 GHz	3-300 GHz	Up to 1 THz
Max. channel bandwidth	100 MHz	1 GHz	100 GHz
Mobility	Up to 350 km/h	Up to 500 km/h	Up to 1000 km/h
Architecture	MIMO	Massive MIMO	Intelligent surface
Artificial intelligence	No	Partial	Fully
THz communications	No	Very Limited	widely
Satellite integration	No	Partial	Fully

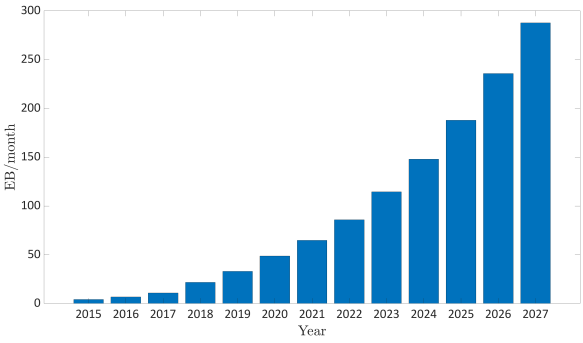

FIGURE 1. Global data traffic from 2015 to 2027 [3].

Although 5G networks offer much higher data rates and lower latency than the previous generations, they may not be able to satisfy the future demands of data rate and latency for some applications [6], [7], [8]. For instance, as more latency-sensitive applications emerge such as self-driving cars, unmanned air vehicles (UAVs), metaverses, etc., the current 5G network may not satisfy the required latencies. Moreover, as the number of connected devices demanding high rates increases, the current 5G network will also struggle to provide high data rate services. Therefore, it is imperative to develop more advanced network protocols or systems to meet future demands.

The sixth-generation (6G) communication network is envisioned to connect trillions of devices and deliver over 10 to 100 times higher data rates than the current 5G network [9]. Additionally, the expected latency for 6G networks is a fraction of a millisecond. Furthermore, 6G networks are expected to support various emerging applications such as virtual and augmented reality, smart cities, intelligent transportation systems, and Industry 4.0, among others, providing a foundation for transformative technological advancements [10]. These applications require high throughput, ultra-reliable low-latency communication (URLLC), and massive machine-type communication (mMTC) [11], [12]. Hence, 6G will need to provide a diverse set of services to support these various applications effectively. However, the development of 6G networks is still in its infancy. Several research efforts are currently underway to explore various solutions, such as new modulation schemes, beamforming techniques, and massive multiple-input and multiple-output (MIMO) systems [13], [14], [15], [16]. Moreover, moving towards higher frequency bands is a potential solution to provide low-latency communications and higher data rates.

Terahertz (THz) band (0.1 to 10 THz) is considered to be one of the key enablers for future 6G cellular networks, promising to provide downlink (DL) data rate of 1 Tbps, see Table 1 [6], [14]. Utilizing THz frequencies in communication systems presents several advantages over traditional wireless communication technologies, such as higher data rates, increased bandwidth, and reduced latency. Compared to low-frequency signals, THz signals can convey more information, enabling faster data transfer rates and allowing for new applications like virtual reality (VR), artificial reality (AR), high resolution imaging, and sensing. Moreover, THz presents different communication applications, including centimeter-level localization, sensing, imaging, and precise positioning [8], [18], [19]. In addition, THz communications systems can be employed in conjunction with new technologies, such as ultra or extreme massive MIMO, three-dimensional (3D) beamforming (vertical and horizontal), and intelligent reflecting surface (IRS) to significantly upgrade the system capacity as shown in Fig. 2 [20], [21], [22]. By tapping into the vast potential of THz frequencies, future wireless communication systems can deliver a truly immersive and high-speed connectivity experience, meeting the evolving demands of emerging applications and paving the way for a connected world of the future [23]. However, despite the enormous potential, the utilization of THz frequencies in communication systems introduces new constraints and challenges. Due to the wider bandwidth and higher operating frequencies of THz communication, various aspects of the communication system need to be carefully considered and addressed that are listed as follows:

- THz channel: The THz communication channel presents a number of challenges that are not typically encountered in conventional low-frequency communication

systems and must be addressed in order to fully leverage the benefits of THz systems. These challenges include additional path-losses resulting from absorption by rain and gas, scattering behavior that can degrade signal quality, and a reduction in multipath propagation [8], [13], [20], [24], [25].

- Radio frequency front-end nonlinearities: Radio frequency (RF) front-end nonlinearities such as phase noise (PN), nonlinear power amplifier (PA), carrier frequency offset (CFO), in-phase and quadrature-phase (I/Q) imbalance, and low resolution analog-to-digital converters (ADCs) can significantly impact the performance of communication systems operating in the THz frequency range. These nonlinearities distort the transmitted signal, leading to errors in the received signal [26], [27], [28], [29], [30], [31], [32], [33]. The most crucial aspect in addressing and mitigating the impact of these nonlinearities is developing an accurate model to represent them.
- Beamforming: Beamforming is another challenge for THz systems that require a large number of antenna elements for successful communication. However, increasing the number of elements presents several hardware and installation limitations [34], [35], [36], [37], [38]. Moreover, the beam blockage and beam squint become more crucial when operating in the THz domain.
- IRS: IRS and THz technologies can significantly improve the performance of wireless communication systems, enabling faster data rates, extended coverage, and increased capacity. However, IRS deploying and positioning, optimization of reflection units, and determining the type (active or passive) can be crucial when operating in THz domain [39], [40], [41], [42], [43].

This paper investigates the aforementioned aspects of a communication system by utilizing the THz band. Unlike other surveys, this paper offers a practical discussion of the potential applications of THz communication, with an emphasis on modeling, design, and implementation. In particular, this paper explores the integration of THz communication with MIMO technologies, as well as emerging technologies such as IRS, hybrid beamforming, and artificial intelligence (AI). The main contributions of this paper are outlined in the following section.

A. CONTRIBUTIONS

The contributions of this work are listed as follows:

1) This paper offers a comprehensive exploration of the key factors influencing THz channels, including atmospheric attenuation, scattering, frequency selectivity, and other relevant aspects. It then introduces the challenges and opportunities associated with these THz characteristics, along with related models, providing a thorough understanding of the complexities involved in THz communication channels.
2) The RF front-end is a crucial aspect of future low-power transceiver design. Therefore, this paper uncovers multiple RF front-end nonlinearities at THz communications with a focus on their significance and modeling. Moreover, MIMO channels along with RF front-end nonlinearities are modeled at the THz frequency band.
3) Popular beamforming techniques are discussed along with their deployment concepts and possible usages in the THz domain. Subsequently, the challenges of operating at ultra-high frequencies are discussed. Moreover, possible solutions to mitigate these shortcomings that affect the throughput and efficiency are reviewed.
4) New and disruptive IRS technologies are introduced for the THz frequency band. The combination of IRS and MIMO technologies in THz wireless networks is explored. Furthermore, a review of state-of-the-art works related to AI and the IRS is also provided.

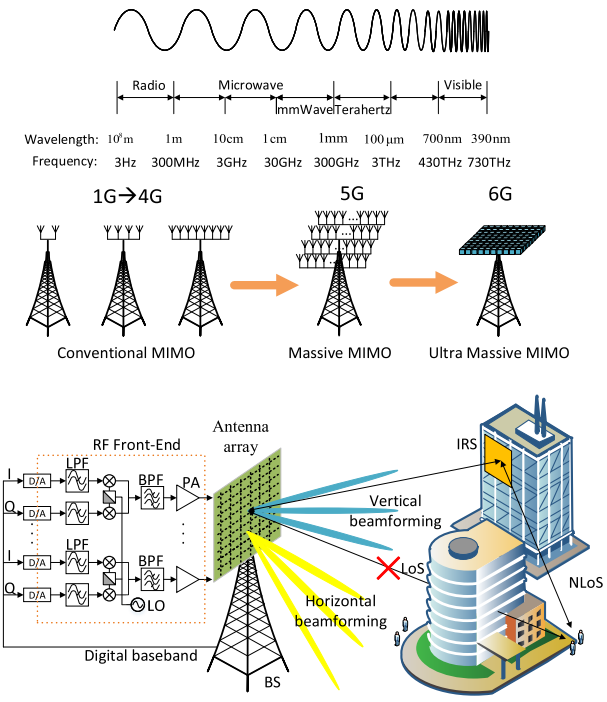

FIGURE 2. Future cellular networks.

The rest of the paper is organized as follows: THz channel characteristics and its modeling are presented in Section II. In Section III, RF front-end nonlinearities at THz frequencies are introduced while focusing on MIMO systems. The principles of beamforming and its significance in THz are presented in Section IV. The application of IRS in MIMO systems at THz frequencies is presented in Section V. Finally, the paper is concluded in Section VI. The overall structural overview of the paper is given in Fig. 3.

II. THz CHANNEL

Due to wider available bandwidth at higher frequencies, THz communication has been regarded as a promising solution for future data-hungry applications [24]. However, as a result

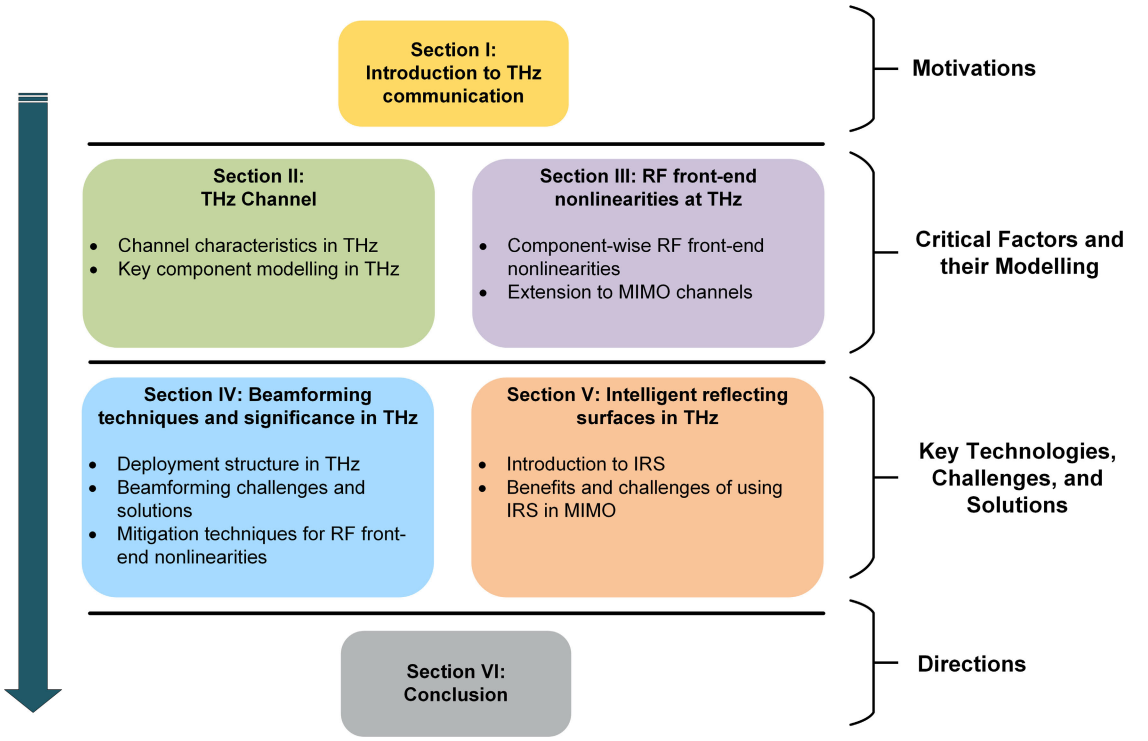

FIGURE 3. Structural overview of the survey paper.

of shorter wavelength (approximately, 3 mm to 30 μm), THz channels have quite different characteristics as opposed to lower microwave frequencies [8], [25] and such distinct channel peculiarities should be appropriately considered for designing THz communication systems. For such purpose, an investigative study is conducted in this section to examine the fundamental characteristics of THz channels and their modeling, as outlined in Section II-A and Section II-B respectively.

A. THz CHANNEL CHARACTERISTICS

This subsection focuses on the unique characteristics of THz channels that deviate from those observed at lower frequencies, or characteristics that exhibit a diminished impact at lower frequencies.

1) FREE-SPACE PATH-LOSS

THz signals are prone to significant free-space path-loss due to spreading loss and atmospheric/molecular loss [13], [20]. The spreading loss occurs from electromagnetic wave expansion in space according to Friis' law, which increases quadratically with the transmission distance and the operating frequency [13]. It can be observed that the free-space path-loss for THz channels can be much greater than 80 dB even for the short-range communication with a distance of 1 meter, see Section II-B1 for more details. Consequently, advanced techniques for extending communication distance are crucial for the stable support of various applications.

2) ATMOSPHERIC ATTENUATION

Besides spreading loss, atmospheric or molecular attenuation leads to higher path-losses at the THz frequency band. The atmospheric or molecular loss occurs as a result of the conversion of THz signal energy into the internal kinetic energy of water vapor molecules as reported in [44]. Additionally, atmospheric attenuation is further comprised of (i) rain attenuation [45] and (ii) gas losses [46]. At frequencies above 10 GHz, the size of raindrops, snow, and hail becomes comparable to the wavelength and, thus, causes significant rain attenuation [47].

Similarly, significant gas losses are observed at higher frequencies as reported in [46] and [48]. Such additional attenuation factors restrict the THz communication to the short distance.

3) SCATTERING AT THz FREQUENCY

At frequencies below 6 GHz, surfaces of buildings, ceilings, and walls are considered to be electrically smooth due to longer wavelength as compared with the height of surface variations [8]. At the frequencies mentioned above, strong specular reflection is the dominant phenomenon and, thus, small-scale scattering can be ignored [8], [25]. At higher frequencies such as millimeter-wave (mmWave) and THz, on the other hand, the wavelength is comparable with the height of surface variations and, therefore, diffuse reflection or specular scattering becomes significant [49], [50]. Fig. 4 briefly illustrates specular reflection and diffuse reflection at

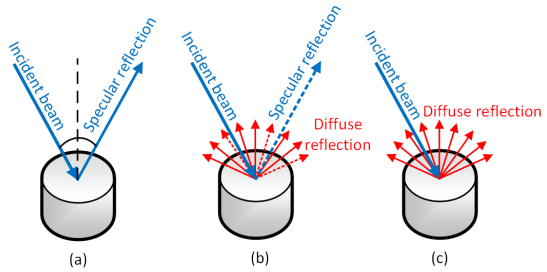

FIGURE 4. Specular reflection at frequencies below 6 GHz, (a) specular and diffuse reflections at THz frequencies, (b) and diffuse reflection at optical frequencies (c).

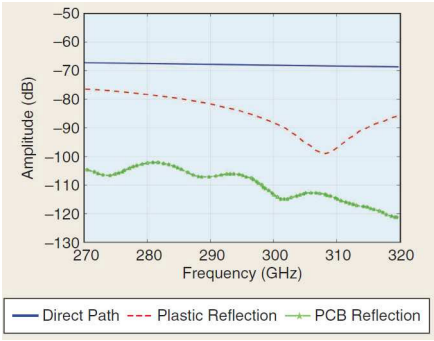

FIGURE 5. Signal attenuation with respect to the operating frequency for (a) the direct path, (b) plastic reflection, and (c) PCB reflection [51].

different frequencies. From the figure, it can be seen that both specular and diffuse reflections can simultaneously occur at THz frequencies as opposed to optical and lower microwave frequency ranges [8], [25], [50]. Because multipath components are mainly determined by specular reflection for typical communication distances, the number of multipath components decreases in general as the operating frequency increases.

4) FREQUENCY SELECTIVITY

As mentioned in Section I, because wider bandwidth might be utilized for THz communication, frequency selectivity can be more significant compared to lower frequency communication. Furthermore, both specular and diffuse reflections can simultaneously occur especially for short-range communication, which are the main ingredients of frequency selectivity at broadband THz channels [25], [50]. These multipath components due to specular and diffuse reflections experience different path delays and, thus, cause constructive and destructive interference at the receiver [8], [51]. Therefore, such a situation leads to significant frequency selectivity for short-range THz communication [52]. Experimental results in [51] show that the frequency selectivity is also dependent on reflective materials. For instance, as seen in Fig. 5, frequency selectivity and signal attenuation are quite different for the direct path only, the single specular reflection from the plastic board, and the single diffuse reflection from the printed circuit board (PCB).

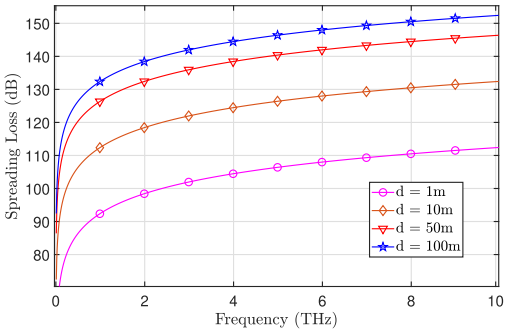

FIGURE 6. Spreading loss with respect to the operating frequency in (1).

5) LIMITED TRANSMIT POWER AND THERMAL NOISE

In general, the output power of a transmitter decreases with higher frequency, and in the near future, it is likely to be only a few decibel-milliwatts[1] [51] for THz communication. Moreover, at higher frequencies, the transmit amplifier has lower efficiency[2] [53]. Due to the aforementioned circumstances, the transmit power cannot be assumed to compensate for severe path-loss in THz communications [54]. Furthermore, thermal noise in a communication channel is proportional to its bandwidth. Therefore, broadband THz channel is subject to having a lower signal-to-noise ratio (SNR) due to both limited output power at the transmitter side and increased thermal noise at the receiver side [55], [56].

B. THz CHANNEL MODELLING

Currently, researches on the measurement and modeling of THz channels have been actively conducted. In this subsection, although somewhat limited, we introduce and discuss several THz channel models reflecting the channel characteristics in Section II-A.

1) SPREADING LOSS AND ATMOSPHERIC ATTENUATION

As mentioned in Section II-A, THz frequency waves experience significant spreading loss as compared with lower frequencies [57]. According to the Friis' law [20], spreading loss is given as

$$L_{\text{spr}}(d, f) = 20 \log_{10}\left(\frac{4\pi d}{\lambda}\right) \text{ dB}, \tag{1}$$

where f (GHz), d (m) and λ (m) are the transmission distance, and wavelength, respectively. Typical values of spreading loss with respect to the operating frequency are indicated in Fig. 6 [47]. It can be seen from the figure that, the spreading loss is greater than 80 dB even for $d = 1$ meter.

Regarding rain and gasses attenuation, ITU-R documents provide concrete models reflecting various environmental parameters, see ITU-R P. 530-17 [45] and ITU-R P.676-12 [46] for more details. Fig. 7 plots the rain attenuation

[1]The transmit power is inversely proportional to the operating frequency by the Friis' law [20].

[2]Current semiconductor technology is unable to deliver high transmission power [51].

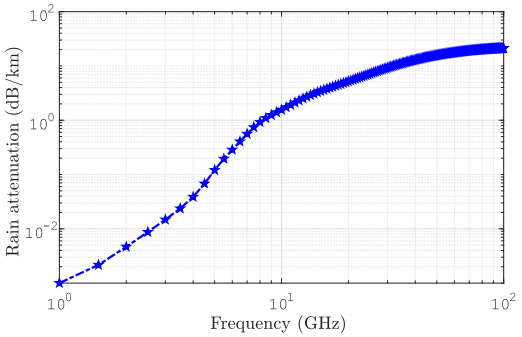

FIGURE 7. Rain attenuation with respect to the operating frequency in ITU-R P. 530-17, where R0.01% is the rain rate (50 mm/h) exceeded for 0.01% of the (average annual year) time while Latitude and longitude indicate the location on the map with corresponding rain rate.

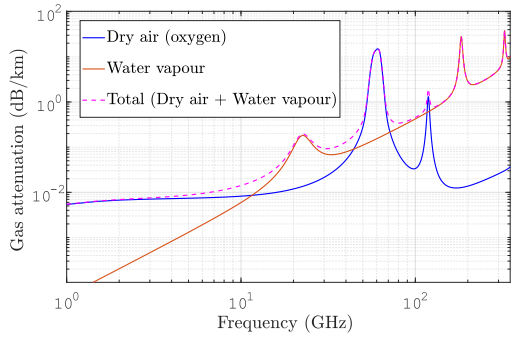

FIGURE 8. Gasses attenuation with respect to the operating frequency in ITU-R P. 676-11, where the total attenuation is the sum attenuation of dry air and water vapour.

simulation in ITU-R P. 530-17 [45]. As seen in the figure, a maximum of 20 dB/km attenuation is observed at the rain rate of 50 mm/h and frequency of 100 GHz. Fig. 8 plots the gasses attenuation simulation in ITU-R P.676-12 [46]. It can be observed that the frequency bands of 183 GHz and 325 GHz receive severe attenuation due to gas losses and, thus, might restrict the communication to a short distance.

2) PATH-LOSS MODELS IN ITU-R P.1411-10 [58]

Under the street canyons scenario, ITU-R documents provide path-loss models that can be used to model mmWave and sub-THz channel path-losses.

a: SITE-GENERAL MODEL

According to the site-general model, the basic transmission loss is given by [58]

$$L_{\mathrm{b}}(d,f) = 10\alpha \log_{10}(d) + \beta + 10\gamma \log_{10}(f) \ \mathrm{dB}, \qquad (2)$$

where, d (m) is the transmission distance, f (GHz) is the operating frequency, α is the path-loss exponent, β indicates the basic transmission loss offset, and γ indicates the basic transmission loss offset associated with frequency. For the site-general model, typical ranges of parameter values are $f \approx 0.8$ to 82 GHz, $\alpha \approx 2.12$ to 5.06, $\beta \approx$ -4.68 to 29.2, and $\gamma \approx 2.02$ to 2.36 depending on line-of-sight (LoS) or non-line-of-sight (NLoS) environments [58].

b: MILLIMETER-WAVE PROPAGATION MODEL

As a site-specific model, the mmWave propagation model in [58] can be used at frequencies 28 and 60 GHz for LoS situations. The basic transmission loss for the case of LoS mmWave propagation is given by

$$L_{\mathrm{LoS}}(d,f) = L_0(f) + 10n \log_{10} \frac{d}{d_0} + L_{\mathrm{rain}}(f) + L_{\mathrm{gas}}(f) \ \mathrm{dB}. \qquad (3)$$

Here, n ($\approx$ 1.9 to 2.21) indicates the basic transmission loss exponent, d (m) is the transmission distance, $L_0(f)$ indicates the basic transmission loss at the reference distance $d_0 = 1$ (m), given by $L_0(f) = 20\log_{10} f - 28$, where f in MHz. Moreover, $L_{\mathrm{rain}}(\cdot)$ and $L_{\mathrm{gas}}(\cdot)$ indicate the rain and gasses attenuation, respectively, see Figs. 7 and 8 for numerical evaluation [45], [46]. Note that (3) can be evaluated for various classes of frequencies, environments, and values of n as indicated in [58, Table 7]. The site general and mmWave propagation models are compared in Fig. 9 at frequencies 28 and 60 GHz. Note that higher path-loss is observed from the mmWave propagation model due to additional rain and gasses losses.

3) SCATTERING MODELS AT THz FREQUENCY

Scattering models are used to predict how signals will behave when they encounter various types of objects and materials. Typically, surfaces of walls, ceilings, and terrain are assumed to be electrically smooth for wavelength greater than 5 cm and, therefore, scattering is negligible for such cases [8]. However, scattering becomes an important phenomenon at mmWave and THz frequencies because the variation of surface height becomes comparable to the wavelength and, thus, causes significant scattering effects [25]. Therefore, such scattered waves need to be considered at mmWave and THz frequencies, especially to evaluate their support for NLoS links. For THz frequencies, the directive scattering model [8], [25] and the Beckmann–kirchhoff scattering model [50], [59] have been widely applied. In addition to these scattering models, ray-tracing channel models have also been developed based on deterministic or statistical methods in [13] and [60]. Specifically, [13] focuses on massive MIMO propagation models and [60] provides an in-depth analysis of channel characteristics, including distance-varying and frequency-selective properties, as well as propagation factors in THz bands.

4) SHADOWING AND THERMAL NOISE

Shadowing is a phenomenon that occurs when a signal is blocked or absorbed by an object, resulting in a reduction of the signal strength at certain locations. At THz frequencies, the wavelength of the signal is much shorter than at lower frequencies. Similar to conventional communication, the log-normal distribution is used to model shadowing at

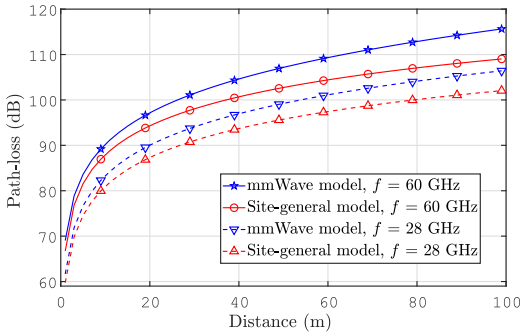

FIGURE 9. Path-loss comparison under the street canyons scenario ITU-R P. 1411-10.

THz communications [61]. The log-normal distribution is defined by Gaussian distribution with mean μ, and standard deviation σ, around the mean path-loss in the logarithmic scale. Moreover, σ is calculated according to the path-loss and is given in [62, Table 7.4.1-1]. It has been reported that this shadowing model is valid for frequencies 0.5 to 100 GHz [62].

The noise in THz originated from two main sources, i.e., conventional thermal noise (or system noise) and frequency-dependent molecular absorption noise [63]. Besides molecular absorption noise, thermal noise is a major contributor to the total noise at THz [64]. The thermal noise power at THz can be approximated as white Gaussian noise and can be given as

$$P_N = 10\log_{10}(K_B T B), \tag{4}$$

where K is the Boltzmann's constant, T is the temperature, and B is the bandwidth [65], [66].

III. RF FRONT-END NONLINEARITIES AT THz

Wireless transceivers operating in the THz frequency spectrum are susceptible to intricate distortions, resulting from the combined effects of several factors such as PN, nonlinear PA, I/Q imbalance, CFO, and low resolution ADCs as shown in Fig. 10 [26], [27], [28], [29], [30], [31], [32], [33]. The aforementioned impairments are caused by (i) higher operating frequency (mmWave/THz) and (ii) low cost transceivers [26], [67]. Such RF front-end impairments limit the system performance by causing in-band and out-of-band interference, higher error vector magnitude, and significant adjacent channel leakage ratio [33]. This section explores the RF front-end impairments along with their signal models. In particular, the effects of these impairments on state-of-the-art communication technologies are discussed.

A. PHASE NOISE

Note that PN in the THz frequency range is a critical consideration in high-precision signal processing. This phenomenon refers to the deviation in the phase of a sinusoidal waveform and is caused by fluctuations in the local oscillator (LO) frequency [68]. More specifically, PN causes the signal to spread in the frequency domain and, hence, results in inter-channel interference [26]. Therefore, signal spreading due to PN injects the interfering signal into signal bandwidth which degrades system performance (see Fig. 11). Thus, accurate modeling and mitigation of PN are crucial for the development of robust THz communication and sensing systems. Next, we discuss the characteristics and modeling of PN in MIMO channels.

1) PN IN MIMO CHANNELS

For the $N \times M$ traditional point-to-point MIMO channel, the received signal vector at time t is given as [69]

$$\mathbf{y}[t] = \mathbf{H}[t]\mathbf{x}[t] + \mathbf{n}[t], \tag{5}$$

where $\mathbf{H} \in \mathbb{C}^{N\times M}$ denotes the MIMO channel matrix, $\mathbf{x} \in \mathbb{C}^{M\times 1}$ is the transmit signal vector and, $\mathbf{n}$ denotes the AWGN noise vector such that each element follows $\mathcal{CN}\left(0, \sigma_n^2\right)$. If both transmitter and receiver are affected by PN, (5) can be modeled as

$$\mathbf{y}[t] = \Theta[t]\mathbf{H}[t]\Phi[t]\mathbf{x}[t] + \mathbf{n}[t], \tag{6}$$

where

$$\begin{aligned}\Phi[t] &= \text{diag}\left(e^{j\phi_1[t]}, \ldots, e^{j\phi_M[t]}\right),\\ \Theta[t] &= \text{diag}\left(e^{j\theta_1[t]}, \ldots, e^{j\theta_N[t]}\right).\end{aligned} \tag{7}$$

Here, $\Theta \in \mathbb{C}^{N\times N}$ and $\Phi \in \mathbb{C}^{M\times M}$ indicate the PN diagonal matrices at the receiver and transmitter, respectively (see Fig. 12). Next, correlated and uncorrelated PN models with respect to SISO models are discussed. The extension to the MIMO case is straightforwardly given [70], [71].

2) PN MODELING

The PN of an oscillator generally has two model representations: an uncorrelated model and a correlated model. The uncorrelated model is simpler but less accurate and arises from white noise sources such as thermal noise and shot noise within the oscillator circuitry. The correlated model, on the other hand, is more accurate and results from white and colored noise sources (e.g., flicker noise).

- Uncorrelated PN model
  The uncorrelated model is relatively simple and only describes the white PN floor. However, the accuracy of this model is not as that of the correlated model. Nevertheless, it is shown that the uncorrelated model is suitable for sub-THz systems [70]. The uncorrelated PN at the transmitter side can be expressed by truncated Gaussian distribution as $\phi[t] = \mathcal{N}\left(0, \sigma_{\phi_g}^2\right)$.
  Since the phase $\phi[t]$ is naturally bounded by $(0, 2\pi]$, therefore, the resulting distribution is called truncated Gaussian distribution. Similar to the transmitter side, PN at the receiver side is expressed as $\theta[t] = \mathcal{N}\left(0, \sigma_{\theta_g}^2\right)$.
- Correlated PN model
  The correlated model is widely used for mmWave systems due to its accuracy [72]. It is described by

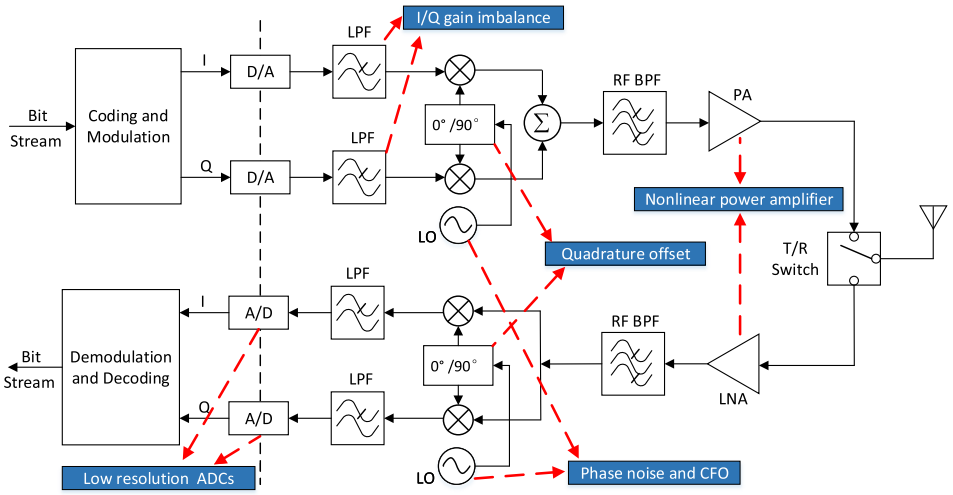

FIGURE 10. Direct conversion transceiver structure and RF front-end nonlinearities.

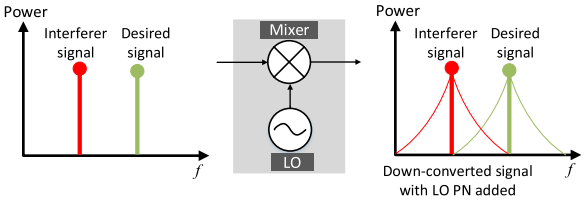

FIGURE 11. LO injected PN introduces spurious signals that interfere within the bandwidth of the desired signal.

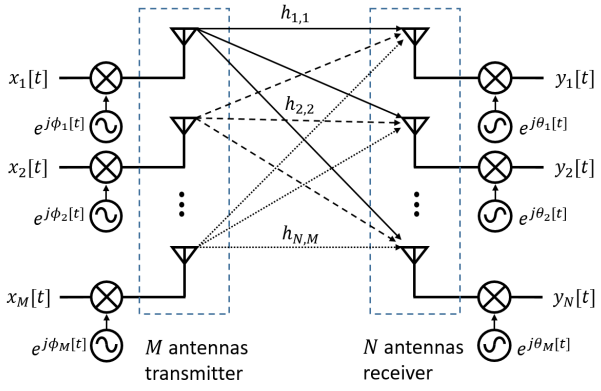

FIGURE 12. PN in MIMO systems.

both uncorrelated contributions such as white PN floor and also correlated PN contributions such as colored PN floor as well. Generally, when the free-running oscillators are stabilized by means of phase-locked loop (PLL), PN is generated which is lower in magnitude and consequently modeled as zero mean, stationary, finite power random process [71]. Moreover, PLL works as a high-pass filter for free-running oscillators' PN and, thus, suppresses PN below a certain cut-off frequency [73]. While employing PLL, the cumulative and correlated nature of oscillators' PN, $\phi[t]$, can be modeled by superposition of the Wiener process, $\phi_w[t]$, and Gaussian process, $\phi_g[t]$, as [70], [71], [74]

$$\phi[t] = \phi_w[t] + \phi_g[t], \tag{8}$$

where $\phi_g[t] \sim \mathcal{N}(0, \sigma^2_{\phi_g})$ is caused by the thermal noise in the oscillator. Further, $\phi_w[t]$ is given as

$$\phi_w[t] = \phi_w[t-1] + \Delta[t], \tag{9}$$

where $\Delta_w[t] \sim \mathcal{N}(0, \sigma^2_{\phi_w})$ denotes the Wiener increment. Noted that as $\sigma^2_{\phi_w}$ increases, the probability of wrapping also increases. For wireless transceivers, the value of $\sigma^2_{\phi_w}$ typically falls within a range where the deviation $\Delta[t]$ can be well approximated by a Gaussian random variable.

B. NONLINEAR POWER AMPLIFIER

For mmWave/THz frequencies, highly power-efficient PAs are typically required at transmitters to overcome (i) significant path-losses, (ii) lower multipath components, and (iii) higher absorption losses [75], [76]. Moreover, future wireless systems require PAs to operate near their saturation to improve power efficiency which, however, leads to significant nonlinear distortion (NLD) [74], [75]. The NLD is further exacerbated by (i) the use of input signals with a higher peak-to-average power ratio and (ii) wider bandwidth allocation at mmWave/THz frequencies [77]. Because of that, significant signal spreading occurs which results in out-of-band distortion. In the following, different nonlinear PA models are discussed while focusing on MIMO systems.

1) NONLINEAR PA MODELLING

In general, nonlinear PAs are categorized into two main groups: frequency-dependent models and frequency-independent models. This categorization is shown in Fig. 13. The frequency-dependent models can be further divided into Saleh's model and Hammerstein–Volterra (HV) series model.

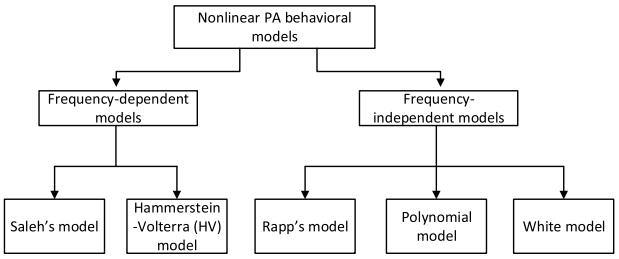

FIGURE 13. Nonlinear PA models.

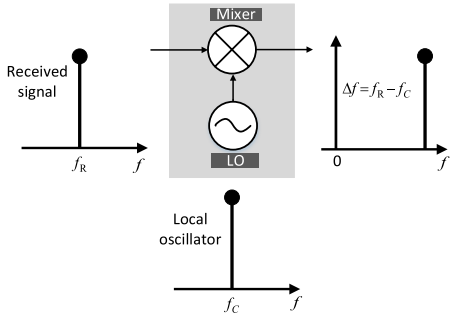

FIGURE 14. CFO representation at the receiver.

On the other hand, the frequency-independent models can be further classified into Rapp's model, the Polynomial model, the White model, and so on.

It is important to note that while both frequency-dependent and frequency-independent models can be used to model nonlinear PAs, frequency-dependent models are generally better at capturing frequency-dependent distortion [76], [78].

2) NONLINEAR PA AND MIMO SYSTEM

As discussed earlier, there are various types of models used for the modeling of nonlinear PAs [27], [28], [79]. Among them, a polynomial model with memory is considered to be the simplest and most widely used model [28]. Considering the same MIMO channel model as of (5) assuming flat fading, the received signal vector is given as [80]

$$\mathbf{y} = \mathbf{H}\left(\Lambda\mathbf{x} + \mathbf{d}\right) + \mathbf{n} \tag{10}$$

using Bussgang's theorem.[3] Here,

$$\Lambda = \text{diag}\left(\alpha_1, \alpha_2, \ldots, \alpha_M\right) \in \mathbb{C}^{M\times M},$$
$$\mathbf{d} = [d_1, d_2, \ldots, d_M]^T \in \mathbb{C}^{M\times 1},$$

i.e., the ith PA output is given by $\alpha_i x_i + d_i$, for all $i \in [1, 2, \ldots, M]$, where α_i is a constant which depends on the PA gain function and its input power [80], and d_i is the distortion noise in the PA such that $d_i \sim \mathcal{N}\left(0, \sigma_{d_i}^2\right)$. Moreover, d_i is uncorrelated with the input signal x_i.

[3]Nonlinear effects on massive MIMO can be characterized by mathematical analysis tools, such as the Bussgang theorem and classical inter-modulation products analysis [75].

C. CARRIER FREQUENCY OFFSET

Note that CFO occurs when the frequency of the carrier signal from the LO in a receiver is not perfectly matched with the incoming signal's carrier frequency [32], [74], [81], which is caused by (i) Doppler shifts and (ii) LO imperfections [74]. The representation of the CFO effect is indicated in Fig. 14, where Δf, f_R, and f_C are the CFO, incoming signal's frequency, and carrier frequency at the receiver's LO, respectively. Note that Δf is the difference between the incoming signal frequency and the frequency at LO i.e., $\Delta f = f_R - f_C$. At higher frequencies such as THz, the impact of CFO on the phase and amplitude of the signal is more pronounced, leading to larger errors in the received signal. Additionally, the sensitivity of THz systems to CFO is often higher due to the wide bandwidth available in the THz range, which can exacerbate the impact of frequency offsets. In the following, we discuss the effect of CFO in MIMO-OFDM systems.

1) CFO IN MIMO-OFDM SYSTEMS

Since CFO is extremely sensitive to OFDM systems, we consider MIMO-OFDM modeling in this section [82]. The received signal for the kth sub-carrier at the mth antenna in the MIMO-OFDM system can be given as

$$y_{m,k}[t] = \mathrm{e}^{j\theta_{\text{CFO}}t}\sum_{m=1}^{M} h_{n,m,k}[t]x_{m,k}[t] + w_{n,k}[t], \tag{11}$$

where, $h_{n,m,k}[t]$ denotes the channel coefficient of the kth sub-carrier with $m \in [1, \ldots, M]$ and $n \in [1, \ldots, N]$ denoting the transmit and receive antenna indices, respectively. Moreover, M and N are the total number of transmit and receive antennas. Furthermore, $x_{m,k}[t]$ is the transmitted signal, and $w_{n,k}[t]$ denotes the additive white Gaussian noise. The term $\mathrm{e}^{j\theta_{\text{CFO}}t}$ in (11) represent the CFO effect, that causes the phase rotation of each OFDM symbol where $\theta_{\text{CFO}} = 2\pi\left(1 + \frac{N_{cp}}{N_{sub}}\right)\epsilon$, where N_{cp} and N_{sub} indicate the number of cyclic prefix and sub-carriers, respectively and ϵ represent the normalized CFO effect due to mobility [82], [83].

D. I/Q IMBALANCE

The amplitudes and phases of the two physical signal branches (in-phase (I) and quadrature-phase (Q)) typically differ to some extent due to imperfections in the analog front-end components such as mixers and filters. This phenomenon is commonly known as the I/Q imbalance problem [84]. It causes modulation distortion, signal spreading, and wide-spectrum sidelobes.

Ideally, I and Q branches must have equal amplitude and 90° phase difference [85]. However, non-ideal low pass filter, 90° phase shifter, and mixers at the transmitter and receiver lead to mismatches in I and Q branches and, thus causes I/Q imbalance [85]. I/Q imbalance caused by a low pass filter is termed as I/Q gain imbalance (or amplitude imbalance), while I/Q imbalance caused by non-ideal 90° phase shifter is termed

as quadrature offset. I/Q gain imbalance and quadrature offset are highlighted in Fig. 10.

In general, the phenomenon of I/Q imbalance can be represented through two distinct models, namely symmetrical and asymmetrical. In the symmetrical approach, both I and Q branches are subjected to identical levels of phase and amplitude errors, with each branch experiencing half of the total error. On the other hand, the asymmetrical approach involves modeling the I branch as perfect, while incorporating the errors solely in the Q branch [86], [87], [88]. However, it has been observed that the symmetrical model can be derived from the asymmetrical one using a linear transformation comprising a rotation matrix and a scaling factor. This transformation allows for the conversion of the asymmetrical model to its symmetrical counterpart. Therefore, in the next section, we present asymmetrical I/Q imbalance modeling with MIMO systems.

1) I/Q IMBALANCE IN MIMO SYSTEMS

Assume the point-to-point MIMO with flat fading as seen in (5). Considering I/Q imbalance at the transmitter side, the transmit signal vector can be modeled as

$$\mathbf{x} = \mathbf{G}_1\mathbf{s} + \mathbf{G}_2\mathbf{s}^*, \tag{12}$$

where

$$\mathbf{G}_1 = \begin{bmatrix} g_{1,1} & \dots & 0 \\ \vdots & \ddots & \\ 0 & \dots & g_{1,M} \end{bmatrix}, \mathbf{G}_2 = \begin{bmatrix} g_{2,1} & \dots & 0 \\ \vdots & \ddots & \\ 0 & \dots & g_{2,M} \end{bmatrix}.$$

Here, $g_{1,i} = \frac{1+\epsilon_i e^{j\psi_i}}{2}$ and $g_{2,i} = \frac{1-\epsilon_i e^{j\psi_i}}{2}$, for all $i \in [1, 2, \dots, M]$ with ϵ_i and ψ_i representing the amplitude and phase mismatch, respectively. The received signal vector in the presence of the receiver-side I/Q imbalance is expressed as

$$\mathbf{z} = \mathbf{K}_1\mathbf{y} + \mathbf{K}_2\mathbf{y}^*, \tag{13}$$

where

$$\mathbf{K}_1 = \begin{bmatrix} k_{1,1} & \dots & 0 \\ \vdots & \ddots & \\ 0 & \dots & k_{1,N} \end{bmatrix}, \mathbf{K}_2 = \begin{bmatrix} k_{2,1} & \dots & 0 \\ \vdots & \ddots & \\ 0 & \dots & k_{2,N} \end{bmatrix}.$$

Here, $k_{1,i} = \frac{1+\zeta_i e^{j\varphi_i}}{2}$ and $k_{2,i} = \frac{1-\zeta_i e^{j\varphi_i}}{2}$, for all $i \in [1, 2, \dots, N]$ with ζ_i and φ_i representing the amplitude an phase mismatch, respectively. From (12) and (13), we have

$$\mathbf{z} = (\mathbf{K}_1\mathbf{H}\mathbf{G}_1 + \mathbf{K}_2\mathbf{H}^*\mathbf{G}_2^*)\mathbf{s} + (\mathbf{K}_1\mathbf{H}\mathbf{G}_2 + \mathbf{K}_2\mathbf{H}^*\mathbf{G}_1^*)\mathbf{s}^* + \mathbf{K}_1\mathbf{n} + \mathbf{K}_2\mathbf{n}^*. \tag{14}$$

E. LOW RESOLUTION ADCs

Besides I/Q imbalance and PAs, ADCs are considered the most power-consuming components [89]. ADC's cost and power consumption grow significantly with (i) the number of quantization bits and (ii) higher sampling rates required at wider bandwidths [89]. Moreover, in MIMO systems, the cost further increases dramatically due to large antenna arrays and many ADCs' employment. Therefore, in practice, low resolution ADCs (i.e., 1-3 bits ADCs) are employed for large-scale MIMO systems that provide a good tradeoff between the energy efficiency and spectral efficiency [90], [91], [92]. In the next section, we provide the modeling of low resolution ADCs in MIMO systems.

1) LOW RESOLUTION ADC IN MIMO SYSTEMS

Considering the same MIMO channel as in (5) with flat fading, the quantized signal after one-bit ADCs can be represented as [89]

$$\mathbf{r} = Q(y) = Q(\mathbf{H}\mathbf{x} + \mathbf{n}), \tag{15}$$

where $Q(\cdot)$ indicates the one-bit quantization operation and is applied separately to real and imaginary parts of the signal given by

$$Q(\cdot) = \frac{1}{\sqrt{2}}(\text{sign}(\Re(\cdot)) + j\text{sign}(\Im(\cdot))). \tag{16}$$

Hence, the one-bit quantization set will then be $\mathcal{R} = \frac{1}{\sqrt{2}}\{1 + j, 1 - j, -1 + j, -1 - j\}$ which is equivalent to QPSK constellation points.

IV. BEAMFORMING AND ITS SIGNIFICANCE IN THz

Moving up the frequencies in the RF spectrum brings several challenges along with benefits. For THz, the wavelength shortens up to a sub-millimeter which also makes the size of the antenna element (fractions of wavelength) small [34], [35], [36]. Hence, the use of the massive number of antennas for THz will be the unavoidable option to grasp the advantages provided by high frequencies. It is worth noting that with the use of a massive number of antenna elements (i.e., more than thousands for THz), a highly directive beam can be generated also termed as pencil beam [37], [38], [93], and [94]. The severe inherited path-loss effects in THz can be compensated with the aid of such a pencil beam.

A. EXTREME MASSIVE MIMO TECHNOLOGIES

Extreme massive MIMO or ultra-massive MIMO is a promising technology that involves the use of a large number of antennas (usually more than 1024 antennas) at both the transmit and receive ends to achieve high data rates and enhance system performance [95]. Since the signals in the THz band face severe propagation losses (discussed in Section II), and are sub-millimeter wavelength sized, that makes the effective areas of antennas small and hence paving the way for extreme massive MIMO technologies. Extreme massive MIMO happens to be the most suitable option to increase the effective transmit/receive area and to mitigate the propagation loss.

Despite the potential benefits, the implementation of extreme massive MIMO for THz communication systems faces several technical challenges. The high cost of integrating a large number of antennas imposes a significant

challenge. Furthermore, the signal processing algorithms required for massive MIMO in THz systems are computationally demanding, requiring high-performance hardware to implement effectively.

The future 6G wireless communication systems are envisioned to leverage THz frequency bands to provide extremely high data rates, low-latency, and massive connectivity. In order to fulfill these requirements, extreme massive MIMO technologies seem to be a basic building block of the THz communication system. The work on 6G and extreme massive MIMO has already been started and researchers all around the world are focusing on the THz extreme MIMO channel estimation, spatial multiplexing, spectral efficiency, and other related issues [96], [97], [98], [99], [100]. The typical number of antennas for extreme massive MIMO can reach up to tens of thousands [100]. Therefore, the conventional beamforming (digital and analog) schemes could not able to meet the demands due to their limitations. For instance, in digital beamforming, the extreme massive MIMO implementation complexity is exceptionally large since each antenna requires a dedicated RF-chain [101]. Alternatively, a conventional analog beamforming scheme is also not feasible in terms of spectral efficiency since it is only able to transmit a single stream [102], [103].

To address the limitations of both architectures, hybrid beamforming has been considered as a viable solution. By utilizing a limited number of RF-chains, hybrid beamforming offers a balance between fully digital and analog beamforming. The details will be discussed in the subsequent sections.

B. HYBRID BEAMFORMING

In order to overcome the challenges associated with conventional beamforming architectures discussed earlier, a possible solution is the adoption of hybrid beamforming architecture [104], [105], [106], [107], [108], [109]. In a general hybrid beamforming transmitter structure with M antennas and M_{RF} RF-chains, the input vector $\mathbf{x} \in \mathbb{C}^{M\times 1}$ is constructed as [110]

$$\mathbf{x} = \mathbf{F}_{RF}\mathbf{F}_{BB}\mathbf{s}, \tag{17}$$

where $\mathbf{s} \in \mathbb{C}^{L\times 1}$ represents number of streams such that $\mathbb{E}[\mathbf{s}\mathbf{s}^H] \leq \frac{P}{L}\mathbf{I}_L$ with $L \leq M_{RF}$ denotes the number of streams. $\mathbf{F}_{RF}$ is the $M \times M_{RF}$ transmit analog beamforming matrix and $\mathbf{F}_{BB}$ is the $M_{RF} \times L$ digital beamforming matrix such that $\|\mathbf{F}_{RF}\mathbf{F}_{BB}\|^2 \leq L$.

Mainly, there are two types of hybrid beamforming; one is fully-connected and the other is sub-connected which are described in detail as follows.

1) FULLY-CONNECTED STRUCTURES

Fully-connected is a very popular hybrid beamforming structure because of its near-optimal performance [110]. It contains few RF-chains as compared to the total number of antennas. Here, each RF-chain is connected to all the antennas with the help of phase shifters as shown in Fig. 15. As can be seen from the figure, the baseband digital module is implemented to control the spatial streams and to tackle the interference among them in the digital domain. For the fully-connected structure, a single RF-chain can control the entire set of antennas. Hence, it has a more degree of freedom to beamform the signal energy toward the desired directions. From (17), the analog beamforming matrix can be given as

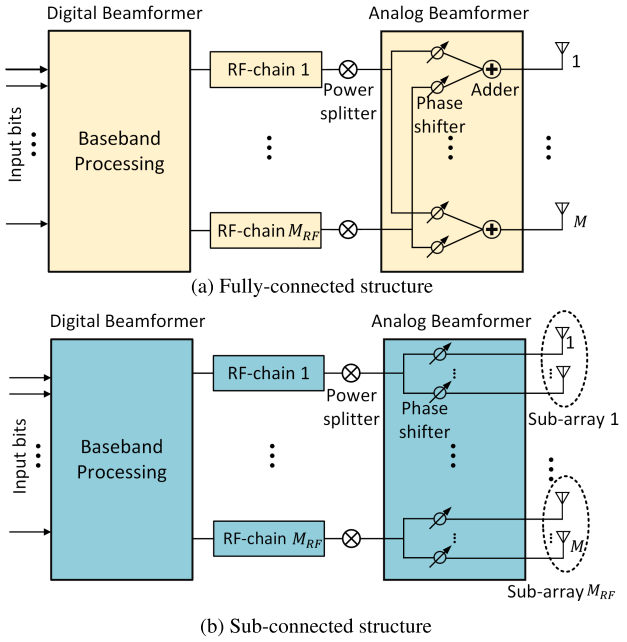

FIGURE 15. Fully-connected and sub-connected hybrid beamforming structures.

$$\mathbf{F}_{RF} = \left[\mathbf{f}_1^{[\mathrm{RF}]}, \mathbf{f}_2^{[\mathrm{RF}]}, \ldots, \mathbf{f}_{M_{RF}}^{[\mathrm{RF}]}\right], \tag{18}$$

where $\mathbf{f}_i^{[\mathrm{RF}]}$ is the $M \times 1$ analog precoding vector associated with the ith RF-chain for $i \in \{1, \ldots, M_{RF}\}$. The main advantage of this architecture is that it can achieve the highest beamforming gain, as all the RF-chains can be used to steer the signal in any direction. Although this architecture is very popular in sub-6 GHz and mmWave frequencies, there are several works in the literature considering the THz domain [104], [105], [106]. In [104], a modified fully-connected structure is proposed for the THz frequencies which can combat the various effects like path-loss of high frequencies. In [105], under the single-user MIMO setup, a new basis vector method is proposed for a wideband OFDM system to mitigate beam squint effects. Although the fully-connected structure can provide near-optimal performance with reduced hardware complexity as compared to the digital beamforming case, this structure still introduces significant hardware complexity due to more phase shifters per antenna (i.e MM_{RF} phase shifters). This can make fully-connected structures not feasible for extreme MIMO techniques operated in the THz band in terms of hardware

cost, power consumption, insertion losses of elements, etc [106].

2) SUB-CONNECTED STRUCTURES

In order to overcome such limitations of fully-connected structures, sub-connected structures have been considered as a feasible option in THz communication. For the sub-connected case, a dedicated set of antennas is assigned to each RF-chain as shown in Fig. 15b. Thereby, decreasing the complexity in terms of phase shifters can further reduce the power consumption of the overall beamforming system. From (17), the analog beamforming matrix for the sub-connected structure is given as

$$\mathbf{F}_{RF} = \text{diag}\left\{\mathbf{f}_1^{[\text{RF}]}, \mathbf{f}_2^{[\text{RF}]}, \ldots, \mathbf{f}_{M_{RF}}^{[\text{RF}]}\right\}, \tag{19}$$

where $\mathbf{f}_i^{[\text{RF}]}$ is the $M_t^{[i]} \times 1$ analog precoding vector of the sub-array associated with the ith RF-chain for $i \in \{1, \ldots, M_{RF}\}$. Here, $M_t^{[i]} \leq M$ denotes the number of antennas in the ith sub-array.

In [106], a detailed comparison between fully-connected and sub-connected structures is provided, demonstrating that the sub-connected structure achieves improved performance for THz in terms of spectral and energy efficiency. A multi-carrier scheme is also introduced for wideband THz systems using the sub-connected structure [104]. A dynamic sub-connected structure with a switching mechanism is introduced in [107] and hybrid precoding algorithms are proposed for THz frequencies to optimize the performance in terms of spectral efficiency and power consumption. A detailed survey about hybrid beamforming techniques is provided in [108], in which various challenges that can arise in THz such as channel sparsity, spherical wave propagation, blockage problem, etc., are discussed. A codebook-based simultaneous beam training method for multiple users under the sub-connected structure to extract the dominant channel information is proposed in [109]. In [111], a wideband multi-carrier hybrid beamforming is considered for THz frequencies in which a two-stage beamforming concept is developed.

C. BEAMFORMING CHALLENGES AND POSSIBLE SOLUTIONS

This subsection discusses several beamforming challenges that arise in THz frequencies.

1) BEAM BLOCKAGE

One of the factors that can affect signal propagation at the THz range is the limited number of available signal paths. At these high frequencies, signals tend to travel in straight lines and are subject to more significant losses due to absorption and scattering. As a result, the number of signal paths available for communication can be significantly reduced (often less than five [104], [106]) and, consequently, beamforming solutions alone are hard to resolve signal blockages due to obstacles. Hence degrading the received signal-to-noise ratio results in reduced coverage. There are a couple of ways to mitigate this issue, one is relay-based signal transmission [112] and the other is to equip IRSs, which is discussed in detail in Section V.

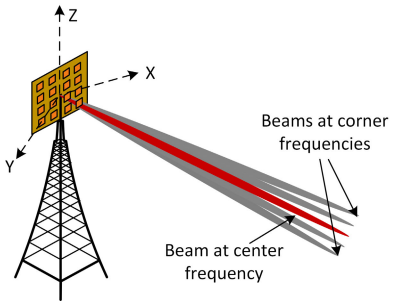

FIGURE 16. Wideband beam squint in THz.

2) POWER CONSUMPTION DUE TO LARGE-SCALE ARRAYS

Despite of utilizing the most feasible option, i.e., sub-connected hybrid structures, power consumption associated with the antenna array with a massive number of antenna elements is still a major challenge due to the use of a massive number of phase shifters (60mW per unit) and power amplifiers (42mW per unit) [107]. One solution that is proposed in the literature is the use of one phase shifter for a group of antenna elements, thereby reducing the number of power consumption devices [111].

3) BEAM SQUINT

Another well-known problem that arises in wideband THz communication systems is the beam squinting issue. In order to attain inherent benefits from THz frequencies, one must move toward the extreme massive MIMO setup. However, increasing the number of antenna elements will create much narrower beams known as pencil beams as shown in Fig. 16, which must be aligned accurately in the desired direction to achieve high data rates [113]. In general, the design of phase shifters is based on the center operating frequency. For the wideband consideration, the direction of such beams may not be accurate due to the difference in the center frequency and the corner frequencies. This phenomenon is called the beam squint effect which can cause severe degradation in the system performance. This beam squint effect can be removed by using the true time delay lines instead of using phase shifters [114] but at the cost of high power consumption (80mW). Several deep learning solutions to overcome the beam squint effects have been proposed in the literature, for example, see [115] and the references therein.

D. MITIGATION APPROACHES FOR THz RF FRONT-END NONLINEARITIES

In Section III, we extensively examined various MIMO models for addressing the nonlinearities present in the RF front-end. In this subsection, we review several mitigation

techniques proposed in the existing literature to combat these nonlinearities.

In [70], index modulation techniques are employed for MIMO and the impact of PN is analyzed when using uniform linear and rectangular antenna arrays. The study showed that employing quadrature phase shift keying (QPSK) schemes with generalized spatial modulation (GSM) can effectively compensate for PN effects, offering a notable gain of up to 5 dB over alternative modulation schemes like double QPSK with GSM (DQPSK-GSM) and 4-ary pulse amplitude modulation with GSM (4PAM-GSM). The authors of [71] analyzed the spectral characteristic of the oscillator and performed measurements of the realistic PN generated by state-of-the-art sub-THz oscillators. They showed that the uncorrelated models are the best choice for sub-THz systems. In [73], the authors presented a comprehensive digital communication system, encompassing PN channel characterization, optimal receiver design, and a robust modulation scheme capable of withstanding PN effects. Their results demonstrated the system's capability to achieve high-rate communication performance.

Numerous studies in the literature tackled the issues related to PA nonlinearities. For example, [77] describes various methods, such as output backoff (OBO) and digital pre-distortion (DPD), that can counteract the nonlinearities caused by PAs. These methods tried to keep the PAs in the linear operating region, avoiding saturation-related distortions. Similarly, [78] discussed techniques to reduce the nonlinear distortions from PAs, with the goal of improving the overall throughput in OFDM-based systems.

To compensate for the effects of I/Q imbalance, several studies have been conducted in the literature. In [85], the authors present a pre-compensation scheme to address nonlinear effects and I/Q imbalances in a low-cost transmitter architecture within a THz system. The study introduced a Maximum Likelihood Estimator, implemented through an alternating estimation algorithm, and derived closed-form expressions for estimating system parameters. The work in [87] proposed a channel and I/Q imbalance coefficients estimation scheme for an uplink multi-user single-input-muliple-output (SIMO) system. The authors also presented an I/Q imbalance compensation scheme based on the estimated I/Q coefficients. In [87], the authors developed novel precoding schemes for massive MIMO systems with I/Q imbalance. The paper introduced a reduced-rank precoding scheme, based on Krylov subspace methods, to lower the computational complexity.

Efficient utilization of low-resolution ADCs is addressed in [92], where an approximate analytical expression for the uplink achievable rate of a massive MIMO system is derived. The study revealed that the degradation in data rate due to low ADC resolution can be mitigated by increasing the number of receiving antennas. In [90], a novel channel estimation approach is presented for an uplink MIMO system equipped with one-bit ADCs at the BS. This approach is applicable to both flat fading and frequency-selective fading channels, demonstrating superior performance when compared to benchmark techniques.

Regarding CFO, [84] introduced a joint clock and frequency synchronization technique aimed at compensating for CFO effects arising from Doppler shifts between the BS and user equipment in an OFDM-based cellular system. Furthermore, [83] addressed CFO and I/Q imbalance concurrently within a MIMO OFDM-based system, proposing an algorithm less susceptible to small CFO errors compared to related studies.

V. INTELLIGENT REFLECTING SURFACES IN THz

In the previous section, we discussed the importance of extreme massive MIMO and hybrid beamforming technologies for the THz systems to realize high data rates up to Tbps in future 6G networks. One of the major challenges for the implementation of such systems is that the reduction of multipath components in THz leads to the dominance of the LoS component. As a result, even a single blockage between the transmitter and the receiver can substantially degrade the communication performance. To design an effective extreme massive MIMO THz-based communication system, IRS (also termed as reconfigurable intelligent surface (RIS) in the literature) is considered to be a promising new technology to overcome the degradation caused by blockages and to provide coverage extension [39], [40]. In general, IRS is a planar structure made up of small, programmable elements that can reflect incoming electromagnetic waves in a controlled manner. In addition to that, these surfaces have many more capabilities such as refraction, absorption, focusing of the incoming signal, polarization alignment, splitting of the incoming signal, analog processing, and collimation as shown in Fig. 17. These surfaces are typically placed between the transmitter and the receiver to enhance the wireless communication link. It can utilize the NLoS path to reflect the incident signals with a controlled phase shift and reflection coefficient for a special direction and signal amplitude [41], when the LoS path is blocked by an obstacle.

During the past few years, numerous works have been carried out considering IRSs as a part of the communication system. In particular, IRS has been extensively used (i) to overcome the severe propagation attenuation, (ii) to upgrade the spectral efficiency, and (iii) to expand the coverage range at THz band frequencies [42], [43]. In general, IRS is equipped with many metamaterial-based passive reconfigurable elements, which are controlled by a central controller (usually controlled by BS). Also, IRS can exploit frequency, phase, polarization, and other characteristics of reflected or refracted electromagnetic waves and, thus, reconfiguration of wireless channels is made possible. Each IRS element can independently control and reflect the incident signal [116]. The structure of a single element of IRS can be seen in Fig. 18. Mathematically the reflected signal from a single IRS element can be expressed by $y = (\beta e^{j\theta})x$, where y and x are the reflected signal and the incident signal, respectively. θ and β represent the phase shift and amplitude of the reflected

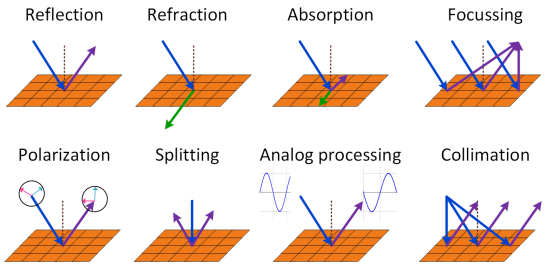

FIGURE 17. IRS capabilities.

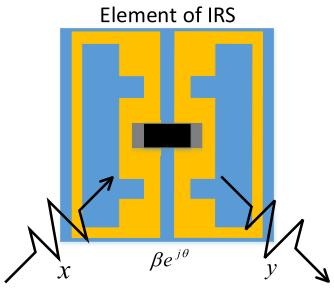

FIGURE 18. Reflection model of an IRS element.

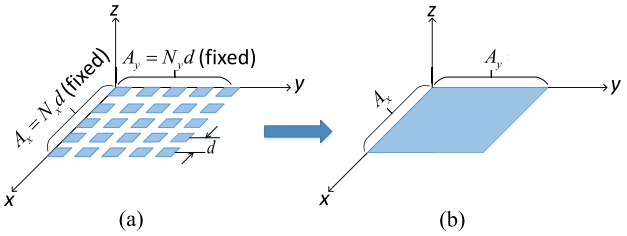

FIGURE 19. Spacing effect between IRS elements (a) discrete IRS (b) continuous aperture (*d* approaches 0).

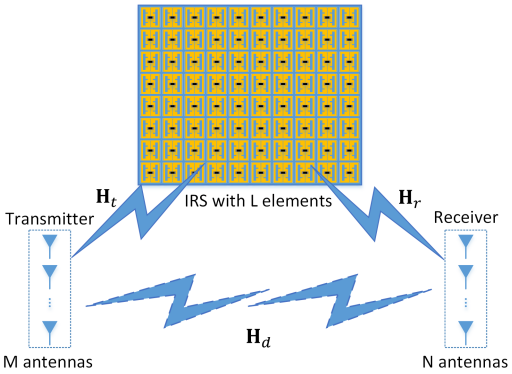

FIGURE 20. System model of IRS-aided MIMO THz communication.

signal, respectively, where $\beta \in [0, 1], \theta \in [0, 2\pi)$ [117]. Specifically, when $\beta = 0$ and $\beta = 1$ represent complete absorption and total reflection of incident signal, respectively. Multiple of these IRS elements is combined in a specific geometry (commonly a planar structure) to form a reflecting surface. These elements are usually placed with a spacing d with each other as shown in Fig. 19. As seen in the figure, when the spacing between elements approaches zero, the ultra-dense IRS surface approximates to the continuous surface [118].

A. IRS AND THz COMMUNICATION

Below are some of the IRS characteristics that make them a feasible solution for THz communication systems.

- Passive: IRS does not require any RF-chains and power amplifiers, therefore, contributing to developing a green economic and reducing energy consumption [118].
- Easy to deploy: The hardware structure of IRS is thin and lightweight, therefore, can be densely and easily deployed on the walls (either, indoors or outdoors).
- Low thermal noise: IRS can achieve passive control of electromagnetic waves, because of the absence of high-power devices (ADCs/DACs, Amplifier, etc.) to process the received signal, hence, no thermal noise is injected.
- Full-band response: Due to its reconfigurable nature, IRS can work at any operating frequency wave.

B. IRS MOTIVATION IN THz

The band of THz can provide plenty of bandwidth to support higher data transmission rates. Despite having a huge advantage in 6G communication, the THz band leads to (i) strong free-space path-losses and water molecules absorption and (ii) the LoS path is easily blocked by an obstacle, leading to unstable communications. Due to the aforementioned disadvantages, making efficient THz communication is a challenging task. Among all the solutions of potential candidates for enhancing current methods of beamforming, IRS technology has been widely recognized as promising in THz wireless networks. IRS can achieve passive beamforming, which can significantly improve the gain of channel compared with active large-scale MIMO antenna array, and achieve low cost and consumption of power. In addition, the transmission distance of THz can be extended at a low cost, especially in indoor application scenarios with high user density and high space shielding, such as stadiums, shopping centers, exhibition centers, and airports, which have great prospects.

C. THz-BASED IRS AND MIMO TECHNIQUES

As mentioned in Section IV-A, massive or extreme massive MIMO has been proven to generate highly directional beams, compensate for its path-loss, achieve efficient active beamforming, and provide high antenna gain to overcome channel loss. However, its capabilities may not be sufficient for the future THz spectrum, because high-frequency information transmission brings higher propagation loss, lower diffraction, and more congestion. As the number of antennas increases, BSs need more RF-chains, which leads to higher complexity and power consumption. Eventually, it greatly increases the cost of the BS and limits the further increase in the scale of massive MIMO antennas. Therefore, IRS can

TABLE 2. Comparison between IRS, relay, and massive MIMO.

Technology	Working principle	Working mode	RF-chain	Cost	Power consumption	Role
IRS	Passive, Reflecting	Full duplex	No	Low	Low	Helper
Relay	Active, Transceived	Half/Full duplex	Yes	High	High	Helper
Massive MIMO	Active, Transceived	Half/Full duplex	Yes	Very high	Very high	Tx/Rx

be integrated into MIMO systems to significantly improve the energy efficiency, spatial diversity and multiplexing of MIMO [119] systems while reducing equipment costs. Table 2 compares IRS with relay and massive MIMO. As can be seen from the table, the loss generated by IRS is very low due to there being no RF-chain. Since IRS only passively reflects signal, there is no self-interfering signal in full-duplex communication as there is in relay devices [120].

Massive MIMO can overcome the severe signal attenuation [121] by employing narrow beams to produce significant beamforming gain and the combination of MIMO and IRS can further enhance the scale of multi-antenna to obtain higher beamforming gain [122]. Assuming the $N \times M$ point-to-point IRS-aided MIMO setup (see Fig. 20), the signal at the receiver is given as

$$\mathbf{y} = (\mathbf{H}_d + \mathbf{H}_r \Sigma \mathbf{H}_t)\, \mathbf{x} + \mathbf{n}, \tag{20}$$

where L denotes the number of IRS elements, $\mathbf{H}_d \in \mathbb{C}^{N\times M}$ denote the direct channel from the transmitter to the receiver, $\mathbf{H}_r \in \mathbb{C}^{N\times L}$ denotes the channel from the IRS to the receiver, and $\mathbf{H}_t \in \mathbb{C}^{L\times M}$ denotes the channel from the transmitter to the IRS. Further, $\Sigma = \text{diag}(\beta_1 e^{j\theta_1}, \ldots, \beta_L e^{j\theta_L})$ is the phase shifts matrix of the IRS, where β_l and θ_l denotes the amplitude and phase shift of the lth reflecting element of the IRS.

D. DEPLOYMENT SCENARIOS FOR THz BASED IRS

Various scenarios have been reported in the literature for the deployment of IRSs in THz communication systems that include outdoor, indoor, and outdoor-to-indoor (O2I) scenarios.

1) OUTDOOR SCENARIO

For outdoor scenarios, IRSs can be deployed on tall building facades to reflect signals from BSs towards users in blind spots, as shown in Fig. 21. Since the LoS path is a necessary component of THz systems, IRSs on buildings, billboards, and poles can provide virtual LoS paths [123], [124]. Furthermore, IRSs can also be deployed on transportation vehicles such as buses, cars, low earth orbit satellites, unmanned air vehicles, etc.

2) INDOOR SCENARIO

Indoor scenarios can be considered as one of the most feasible setups for the IRSs deployment under THz communications

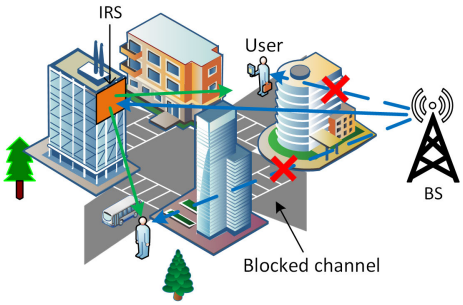

FIGURE 21. Outdoor IRS model.

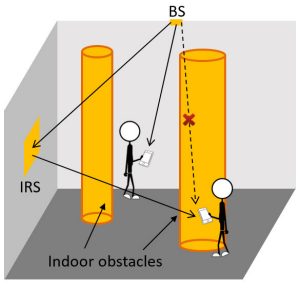

FIGURE 22. Indoor IRS model.

[125], [126], [127]. This is due to the absence of severe path-loss factors, such as rain losses, which tend to affect THz communications. Additionally, user locations in indoor scenarios are typically clustered in specific areas, thereby enabling IRSs to provide more coverage toward densely populated locations. A visual representation of a typical indoor scenario in the presence of blockages is presented in Fig. 22.

3) O2I SCENARIO

The deployment of IRSs under O2I scenarios can also be beneficial in terms of providing the virtual LoS paths to the indoor users incapable of receiving the direct LoS transmissions as shown in Fig. 23. The penetration loss caused by walls is often significant, particularly in modern energy-efficient building architectures, which tend to hinder the incoming signal from passing through them, leading to very weak or no reception for users inside the building [128]. Fig. 23 demonstrates that placing an IRS in the LoS path between the BS and users through a glass window can be highly advantageous.

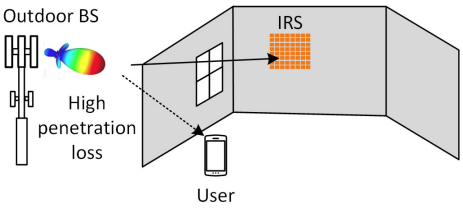

FIGURE 23. O2I IRS model.

E. AI FOR IRS-AIDED THz SYSTEMS

Most of the existing research on IRS largely adheres to the conventional model-driven beamforming design approach, relying heavily on precise and real-time channel information. However, obtaining accurate channel state information for IRS-aided communication systems is quite challenging due to factors such as complexity, cost, and protocol compatibility [129]. To overcome such difficulties, several studies have explored the application of neural networks for channel estimation or beamforming of IRS [130], [131], [132], [133], [134]. One approach is to combine both techniques directly, enabling the learning of beamforming based on received signals. This method, when used in conjunction with deep learning, can extract relevant information from the original data [131]. In particular, the authors in [131] utilized an active sensing strategy to find the beamforming vectors based on the long-short-term memory (LSTM) networks. In [132], a deep neural network (DNN) approach is applied to find the hybrid precoding matrix in IRS-aided THz communication systems. The authors proposed a DNN-based solution by considering the discrete phase shifts of IRS. Similar works have also been proposed in [133] and [134] by considering graph neural networks (GNNs) to optimize the performance of the multi-user MIMO setup in terms of fairness and rate maximization. Overall, AI-based beamforming design strategies offer promising solutions for IRS-aided THz systems, especially in scenarios where channel estimation is difficult or hardware costs are high.

VI. CONCLUSION

In this paper, we presented a comprehensive review of the challenges and solutions in the THz communication systems. We discussed the key characteristics of the THz channels, including free-space path-loss, atmospheric attenuation, scattering, and frequency selectivity, and reviewed the state-of-the-art modeling techniques. Moreover, we investigated the impact of the RF front-end nonlinearities, such as PN, nonlinear PAs, CFO, I/Q imbalance, and low resolution ADCs, and reviewed their modeling for MIMO systems in the light of state-of-the-art literature. We also highlighted the significance of beamforming in the THz communication systems, including extreme massive MIMO technology, hybrid beamforming, fully-connected and sub-connected structures, and identified potential solutions to mitigate the inherent issues. Furthermore, we explored the use of IRS and its potential to improve the THz communication performance through beamforming and signal quality enhancement. Finally, we discussed the potential of IRS with AI-based solutions for optimizing the performance of the THz communication systems.

REFERENCES

[1] Cisco U. *Cisco Annual Internet Report (2018–2023) White Paper*. Accessed: Dec. 20, 2022. [Online]. Available: https://www.cisco.com/c/en/us/solutions/collateral/executive-perspectives/annual-internet-report/white-paper-c11-741490.html

[2] Y. Corre, G. Gougeon, J.-B. Doré, S. Bicaïs, B. Miscopein, E. Faussurier, M. Saad, J. Palicot, and F. Bader, "Sub-THz spectrum as enabler for 6G wireless communications up to 1 Tbit/s," in *Proc. 6G Wireless Summit*, Levi, Finland, Mar. 2019, pp. 1–3.

[3] Ericsson AB. *Traffic Exploration Tool, Interactive Online Tool*. Accessed: Dec. 1, 2022. [Online]. Available: http://www.ericsson.com/TET/trafficView/loadBasicEditor.ericsson8

[4] Capacity Magazine. *Carriers Face 282EB a Month Demand for Mobile Data by 2027*. Accessed: Jun. 20, 2023.[Online]. Available: https://www.capacitymedia.com/article/2a9b81ycm7bxpgne19s74/news/carriers-face-282eb-a-month-demand-for-mobile-data-by-2027

[5] I Union, "IMT traffic estimates for the years 2020 to 2030," Int. Telecommun. Union (ITU), Geneva, Switzerland, Tech. Rep. ITU-R M.2370-0, 2015.

[6] S. Dang, O. Amin, B. Shihada, and M.-S. Alouini, "What should 6G be?" *Nature Electron.*, vol. 3, no. 1, pp. 20–29, Jan. 2020.

[7] Z. Hossain, Q. C. Li, D. Ying, G. Wu, and C. Xiong, "THz channel model for 6G communications," in *Proc. IEEE 32nd Annu. Int. Symp. Pers., Indoor Mobile Radio Commun. (PIMRC)*, Helsinki, Finland, Sep. 2021, pp. 1–7.

[8] T. S. Rappaport, Y. Xing, O. Kanhere, S. Ju, A. Madanayake, S. Mandal, A. Alkhateeb, and G. C. Trichopoulos, "Wireless communications and applications above 100 GHz: Opportunities and challenges for 6G and beyond," *IEEE Access*, vol. 7, pp. 78729–78757, 2019.

[9] P. Yang, Y. Xiao, M. Xiao, and S. Li, "6G wireless communications: Vision and potential techniques," *IEEE Netw.*, vol. 33, no. 4, pp. 70–75, Jul. 2019.

[10] X. You, "Towards 6G wireless communication networks: Vision, enabling technologies, and new paradigm shifts," *Sci. China Inf. Sci.*, vol. 64, no. 1, pp. 1–74, Nov. 2020.

[11] M. Sohaib, J. Jeong, and S.-W. Jeon, "Dynamic multichannel access via multi-agent reinforcement learning: Throughput and fairness guarantees," *IEEE Trans. Wireless Commun.*, vol. 21, no. 6, pp. 3994–4008, Jun. 2022.

[12] S.-W. Jeon and H. Jin, "Online estimation and adaptation for random access with successive interference cancellation," *IEEE Trans. Mobile Comput.*, vol. 22, no. 9, pp. 5418–5433, Sep. 2023.

[13] C. Han and Y. Chen, "Propagation modeling for wireless communications in the terahertz band," *IEEE Commun. Mag.*, vol. 56, no. 6, pp. 96–101, Jun. 2018.

[14] F. Tariq, M. R. A. Khandaker, K.-K. Wong, M. A. Imran, M. Bennis, and M. Debbah, "A speculative study on 6G," *IEEE Wireless Commun.*, vol. 27, no. 4, pp. 118–125, Aug. 2020.

[15] S. H. Chae and S.-W. Jeon, "Integer forcing interference management for the MIMO interference channel," *IEEE Trans. Wireless Commun.*, vol. 22, no. 2, pp. 1101–1115, Feb. 2023.

[16] S. H. Chae, H. W. Kim, and S.-W. Jeon, "Rate splitting-based hybrid beamforming for multi-user downlink cellular networks," *IEEE Trans. Commun.*, to be published.

[17] M. Z. Chowdhury, M. Shahjalal, S. Ahmed, and Y. M. Jang, "6G wireless communication systems: Applications, requirements, technologies, challenges, and research directions," *IEEE Open J. Commun. Soc.*, vol. 1, pp. 957–975, 2020.

[18] Y. Xing and T. S. Rappaport, "Terahertz wireless communications: Co-sharing for terrestrial and satellite systems above 100 GHz," *IEEE Commun. Lett.*, vol. 25, no. 10, pp. 3156–3160, Oct. 2021.

[19] O. Kanhere and T. S. Rappaport, "Position location for futuristic cellular communications: 5G and beyond," *IEEE Commun. Mag.*, vol. 59, no. 1, pp. 70–75, Jan. 2021.

[20] L. Zhang, Y.-C. Liang, and D. Niyato, "6G visions: Mobile ultra-broadband, super Internet-of-Things, and artificial intelligence," *China Commun.*, vol. 16, no. 8, pp. 1–14, Aug. 2019.

[21] H. Elayan, O. Amin, R. M. Shubair, and M.-S. Alouini, "Terahertz communication: The opportunities of wireless technology beyond 5G," in *Proc. Int. Conf. Adv. Commun. Technol. Netw. (CommNet)*, Marrakech, Morocco, Apr. 2018, pp. 1–5.

[22] N. U. Saqib, K. Park, H.-G. Song, and S.-W. Jeon, "3D hybrid beamforming with 2D planar antenna arrays for downlink massive MIMO systems," in *Proc. Int. Conf. Inf. Commun. Technol. Converg. (ICTC)*, Jeju Island, South Korea, Oct. 2021, pp. 616–620.

[23] Z. Chen, X. Ma, B. Zhang, Y. Zhang, Z. Niu, N. Kuang, W. Chen, L. Li, and S. Li, "A survey on terahertz communications," *China Commun.*, vol. 16, no. 2, pp. 1–35, Feb. 2019.

[24] H. Tataria, M. Shafi, A. F. Molisch, M. Dohler, H. Sjöland, and F. Tufvesson, "6G wireless systems: Vision, requirements, challenges, insights, and opportunities," *Proc. IEEE*, vol. 109, no. 7, pp. 1166–1199, Jul. 2021.

[25] S. Ju, S. Shah, M. Javed, J. Li, G. Palteru, J. Robin, Y. Xing, O. Kanhere, and T. S. Rappaport, "Scattering mechanisms and modeling for terahertz wireless communications," in *Proc. IEEE Int. Commun. Conf.*, Shanghai, China, May 2019, pp. 1–7.

[26] A. Mohammadian and C. Tellambura, "RF impairments in wireless transceivers: Phase noise, CFO, and IQ imbalance—A survey," *IEEE Access*, vol. 9, pp. 111718–111791, 2021.

[27] H. Hemesi, A. Abdipour, and A. Mohammadi, "Analytical modeling of MIMO-OFDM system in the presence of nonlinear power amplifier with memory," *IEEE Trans. Commun.*, vol. 61, no. 1, pp. 155–163, Jan. 2013.

[28] M. B. Salman and G. M. Guvensen, "On the effects of PA nonlinearities for hybrid beamforming based wideband massive MIMO systems," in *Proc. IEEE Int. Conf. Commun. (ICC)*, Dublin, Ireland, Jun. 2020, pp. 1–7.

[29] S. Yan, C. Zhang, and Q.-J. Zhang, "Recurrent neural network technique for behavioral modeling of power amplifier with memory effects," *Int. J. RF Microw. Comput.-Aided Eng.*, vol. 25, no. 4, pp. 289–298, May 2015.

[30] D. R. Morgan, Z. Ma, J. Kim, M. G. Zierdt, and J. Pastalan, "A generalized memory polynomial model for digital predistortion of RF power amplifiers," *IEEE Trans. Signal Process.*, vol. 54, no. 10, pp. 3852–3860, Oct. 2006.

[31] J. Zhang, R. Woods, M. Sandell, M. Valkama, A. Marshall, and J. Cavallaro, "Radio frequency fingerprint identification for narrowband systems, modelling and classification," *IEEE Trans. Inf. Forensics Security*, vol. 16, pp. 3974–3987, 2021.

[32] Z. Zhu, H. Leung, and X. Huang, "Challenges in reconfigurable radio transceivers and application of nonlinear signal processing for RF impairment mitigation," *IEEE Circuits Syst. Mag.*, vol. 13, no. 1, pp. 44–65, 1st Quart., 2013.

[33] K. Zhi, C. Pan, H. Ren, and K. Wang, "Uplink achievable rate of intelligent reflecting surface-aided millimeter-wave communications with low-resolution ADC and phase noise," *IEEE Wireless Commun. Lett.*, vol. 10, no. 3, pp. 654–658, Mar. 2021.

[34] I. F. Akyildiz, J. M. Jornet, and C. Han, "Terahertz band: Next frontier for wireless communications," *Phys. Commun.*, vol. 12, pp. 16–32, Sep. 2014.

[35] K. M. S. Huq, J. M. Jornet, W. H. Gerstacker, A. Al-Dulaimi, Z. Zhou, and J. Aulin, "THz communications for mobile heterogeneous networks," *IEEE Commun. Mag.*, vol. 56, no. 6, pp. 94–95, Jun. 2018.

[36] W. Xia, V. Semkin, M. Mezzavilla, G. Loianno, and S. Rangan, "Multi-array designs for mmWave and sub-THz communication to UAVs," in *Proc. IEEE 21st Int. Workshop Signal Process. Adv. Wireless Commun. (SPAWC)*, May 2020, pp. 1–5.

[37] S. A. Hoseini, M. Ding, and M. Hassan, "Massive MIMO performance comparison of beamforming and multiplexing in the terahertz band," in *Proc. IEEE Globecom Workshops (GC Wkshps)*, Singapore, Dec. 2017, pp. 1–6.

[38] C. Chaccour, M. N. Soorki, W. Saad, M. Bennis, and P. Popovski, "Can terahertz provide high-rate reliable low-latency communications for wireless VR?" *IEEE Internet Things J.*, vol. 9, no. 12, pp. 9712–9729, Jun. 2022.

[39] M. Forouzanmehr, S. Akhlaghi, A. Khalili, and Q. Wu, "Energy efficiency maximization for IRS-assisted uplink systems: Joint resource allocation and beamforming design," *IEEE Commun. Lett.*, vol. 25, no. 12, pp. 3932–3936, Dec. 2021.

[40] J. Zhao, "A survey of intelligent reflecting surfaces (IRSs): Towards 6G wireless communication networks," 2019, *arXiv:1907.04789*.

[41] X. Ma, Z. Chen, W. Chen, Z. Li, Y. Chi, C. Han, and S. Li, "Joint channel estimation and data rate maximization for intelligent reflecting surface assisted terahertz MIMO communication systems," *IEEE Access*, vol. 8, pp. 99565–99581, 2020.

[42] Z. Chen, X. Ma, C. Han, and Q. Wen, "Towards intelligent reflecting surface empowered 6G terahertz communications: A survey," *China Commun.*, vol. 18, no. 5, pp. 93–119, May 2021.

[43] C. Huang, Z. Yang, G. C. Alexandropoulos, K. Xiong, L. Wei, C. Yuen, Z. Zhang, and M. Debbah, "Multi-hop RIS-empowered terahertz communications: A DRL-based hybrid beamforming design," *IEEE J. Sel. Areas Commun.*, vol. 39, no. 6, pp. 1663–1677, Jun. 2021.

[44] K. Rikkinen, P. Kyosti, M. E. Leinonen, M. Berg, and A. Parssinen, "THz radio communication: Link budget analysis toward 6G," *IEEE Commun. Mag.*, vol. 58, no. 11, pp. 22–27, Nov. 2020.

[45] *Propagation Data and Prediction Methods Required for the Design of Terrestrial Line-of-Sight Systems*, document Recommendation ITU-R P.530-17, 2017.

[46] *Attenuation by Atmospheric Gases and Related Effects*, document Recommendation ITU-R P.676-12, 2019.

[47] S. Liu, X. Yu, R. Guo, Y. Tang, and Z. Zhao, "THz channel modeling: Consolidating the road to THz communications," *China Commun.*, vol. 18, no. 5, pp. 33–49, May 2021.

[48] M. E. Shawon, M. Z. Chowdhury, M. B. Hossen, M. F. Ahmed, and Y. M. Jang, "Rain attenuation characterization for 6G terahertz wireless communication," in *Proc. Int. Conf. Artif. Intell. Inf. Commun. (ICAIIC)*, Jeju Island, South Korea, Apr. 2021, pp. 416–420.

[49] A. A. Goulianos, A. L. Freire, T. Barratt, E. Mellios, P. Cain, M. Rumney, A. Nix, and M. Beach, "Measurements and characterisation of surface scattering at 60 GHz," in *Proc. IEEE 86th Veh. Technol. Conf. (VTC-Fall)*, Toronto, ON, Canada, Sep. 2017, pp. 1–5.

[50] F. Sheikh, Y. Gao, and T. Kaiser, "A study of diffuse scattering in massive MIMO channels at terahertz frequencies," *IEEE Trans. Antennas Propag.*, vol. 68, no. 2, pp. 997–1008, Feb. 2020.

[51] B. Peng, K. Guan, A. Kuter, S. Rey, M. Patzold, and T. Kuerner, "Channel modeling and system concepts for future terahertz communications: Getting ready for advances beyond 5G," *IEEE Veh. Technol. Mag.*, vol. 15, no. 2, pp. 136–143, Jun. 2020.

[52] H. Yuan, N. Yang, K. Yang, C. Han, and J. An, "Hybrid beamforming for MIMO-OFDM terahertz wireless systems over frequency selective channels," in *Proc. IEEE Global Commun. Conf. (GLOBECOM)*, Abu Dhabi, United Arab Emirates, Dec. 2018, pp. 1–6.

[53] Z. Wang, P.-Y. Chiang, P. Nazari, C.-C. Wang, Z. Chen, and P. Heydari, "A 210 GHz fully integrated differential transceiver with fundamental-frequency VCO in 32 nm SOI CMOs," in *IEEE Int. Solid-State Circuits Conf. (ISSCC) Dig. Tech. Papers*, San Francisco, CA, USA, Feb. 2013, pp. 136–137.

[54] Y. Xing, T. S. Rappaport, and A. Ghosh, "Millimeter wave and sub-THz indoor radio propagation channel measurements, models, and comparisons in an office environment," *IEEE Commun. Lett.*, vol. 25, no. 10, pp. 3151–3155, Oct. 2021.

[55] J. M. Eckhardt, C. Herold, B. Friebel, N. Dreyer, and T. Kürner, "Realistic interference simulations in a data center offering wireless communication at low terahertz frequencies," in *Proc. Int. Symp. Antennas Propag. (ISAP)*, Taipei, Taiwan, Oct. 2021, pp. 1–2.

[56] K. Guan, H. Yi, D. He, B. Ai, and Z. Zhong, "Towards 6G: Paradigm of realistic terahertz channel modeling," *China Commun.*, vol. 18, no. 5, pp. 1–18, May 2021.

[57] W. Hedhly, O. Amin, B. Shihada, and M.-S. Alouini, "A power saving scheme for IEEE 802.15.3d THz wireless communication links," *IEEE Trans. Mobile Comput.*, vol. 22, no. 4, pp. 1912–1921, Apr. 2023.

[58] *Propagation Data and Prediction Methods for the Planning of Short-Range Outdoor Radio Communication Systems and Radio Local Area Networks in the Frequency Range 300 MHz to 100 GHz*, document Recommendation ITU-R P.1411-10, 2019.

[59] F. Sheikh and T. Kaiser, "A modified beckmann-kirchhoff scattering model for slightly rough surfaces at terahertz frequencies," in *Proc. IEEE Int. Symp. Antennas Propag. USNC-URSI Radio Sci. Meeting*, Atlanta, GA, USA, Jul. 2019, pp. 2079–2080.

[60] C. Han, A. O. Bicen, and I. F. Akyildiz, "Multi-ray channel modeling and wideband characterization for wireless communications in the terahertz band," *IEEE Trans. Wireless Commun.*, vol. 14, no. 5, pp. 2402–2412, May 2015.

[61] E. N. Papasotiriou, A.-A.-A. Boulogeorgos, K. Haneda, M. F. de Guzman, and A. Alexiou, "An experimentally validated fading model for THz wireless systems," *Sci. Rep.*, vol. 11, no. 1, pp. 1–14, Sep. 2021.

[62] *Technical Specification Group Radio Access Network; Study on Channel Model for Frequencies From 0.5 to 100 GHz*, 3GPP, document TR 38.901, 2019.

[63] J. M. Jornet and I. F. Akyildiz, "Channel modeling and capacity analysis for electromagnetic wireless nanonetworks in the terahertz band," *IEEE Trans. Wireless Commun.*, vol. 10, no. 10, pp. 3211–3221, Oct. 2011.

[64] C. Han and I. F. Akyildiz, "Distance-aware bandwidth-adaptive resource allocation for wireless systems in the terahertz band," *IEEE Trans. Terahertz Sci. Technol.*, vol. 6, no. 4, pp. 541–553, Jul. 2016.

[65] T. Schneider, A. Wiatrek, S. Preussler, M. Grigat, and R.-P. Braun, "Link budget analysis for terahertz fixed wireless links," *IEEE Trans. Terahertz Sci. Technol.*, vol. 2, no. 2, pp. 250–256, Mar. 2012.

[66] J. Kokkoniemi, A.-A.-A. Boulogeorgos, M. Aminu, J. Lehtomäki, A. Alexiou, and M. Juntti, "Impact of beam misalignment on THz wireless systems," *Nano Commun. Netw.*, vol. 24, May 2020, Art. no. 100302.

[67] A. Mohammadian, C. Tellambura, and G. Y. Li, "Deep learning LMMSE joint channel, PN, and IQ imbalance estimator for multicarrier MIMO full-duplex systems," *IEEE Wireless Commun. Lett.*, vol. 11, no. 1, pp. 111–115, Jan. 2022.

[68] C. Li, A. Sezgin, and Z. Han, "On the impact of oscillator phase noise in an IRS-assisted MISO TDD system," in *Proc. 25th Int. ITG Workshop Smart Antennas*, Biot, France, Nov. 2021, pp. 1–6.

[69] M. Saad, F. Bader, A. C. Al Ghouwayel, H. Hijazi, N. Bouhel, and J. Palicot, "Generalized spatial modulation for wireless terabits systems under sub-THz channel with RF impairments," in *Proc. IEEE Int. Conf. Acoust., Speech Signal Process. (ICASSP)*, Barcelona, Spain, May 2020, pp. 5135–5139.

[70] S. Bicais and J.-B. Dore, "Phase noise model selection for sub-THz communications," in *Proc. IEEE Global Commun. Conf. (GLOBECOM)*, Honolulu, HI, USA, Dec. 2019, pp. 1–6.

[71] L. Piazzo and P. Mandarini, "Analysis of phase noise effects in OFDM modems," *IEEE Trans. Commun.*, vol. 50, no. 10, pp. 1696–1705, Oct. 2002.

[72] S. Bicaïs and J.-B. Doré, "Design of digital communications for strong phase noise channels," *IEEE Open J. Veh. Technol.*, vol. 1, pp. 227–243, 2020.

[73] M. R. Khanzadi, D. Kuylenstierna, A. Panahi, T. Eriksson, and H. Zirath, "Calculation of the performance of communication systems from measured oscillator phase noise," *IEEE Trans. Circuits Syst. I, Reg. Papers*, vol. 61, no. 5, pp. 1553–1565, May 2014.

[74] A. Mohammadi and F. M. Ghannouchi, *RF Transceiver Design for MIMO Wireless Communications*. New York, NY, USA: Springer, 2012.

[75] S. Teodoro, A. Silva, R. Dinis, and A. Gameiro, "Performance impact of nonlinear amplification in massive MIMO mmWave systems," in *Proc. IEEE 89th Veh. Technol. Conf. (VTC-Spring)*, Kuala Lumpur, Malaysia, Apr. 2019, pp. 1–5.

[76] X. Yang, M. Matthaiou, J. Yang, C.-K. Wen, F. Gao, and S. Jin, "Hardware-constrained millimeter-wave systems for 5G: Challenges, opportunities, and solutions," *IEEE Commun. Mag.*, vol. 57, no. 1, pp. 44–50, Jan. 2019.

[77] P. K. Singya, N. Kumar, and V. Bhatia, "Mitigating NLD for wireless networks: Effect of nonlinear power amplifiers on future wireless communication networks," *IEEE Microw. Mag.*, vol. 18, no. 5, pp. 73–90, Jul. 2017.

[78] P. Jantunen, "Modelling of nonlinear power amplifiers for wireless communications," M.S. thesis, Dept. Elect. Telecommun. Eng., Aalto Univ., Finland, 2004. [Online]. Available: http://legacy.spa.aalto.fi/sig-legacy/spit/publications/2004t1.pdf

[79] H. Ku, M. D. McKinley, and J. S. Kenney, "Quantifying memory effects in RF power amplifiers," *IEEE Trans. Microw. Theory Techn.*, vol. 50, no. 12, pp. 2843–2849, Dec. 2002.

[80] M. Fozooni, M. Matthaiou, E. Bjornson, and T. Q. Duong, "Performance limits of MIMO systems with nonlinear power amplifiers," in *Proc. IEEE Global Commun. Conf. (GLOBECOM)*, San Diego, CA, USA, Dec. 2015, pp. 1–7.

[81] Z. Mokhtari and R. Dinis, "Residual CFO effect on uplink sum-rate of cell free massive MIMO systems," in *Proc. IEEE 94th Veh. Technol. Conf. (VTC-Fall)*, Norman, OK, USA, Sep. 2021, pp. 1–6.

[82] M. Sandell, E. Tsimbalo, S. Jardak, D. Uchida, K. Akita, D. Yoda, T. Kawaguchi, and M. Sano, "Estimation of wideband IQ imbalance in MIMO OFDM systems with CFO," *IEEE Trans. Wireless Commun.*, vol. 20, no. 9, pp. 5821–5830, Sep. 2021.

[83] H. Lee and J. Lee, "Joint clock and frequency synchronization for OFDM-based cellular systems," *IEEE Signal Process. Lett.*, vol. 18, no. 12, pp. 757–760, Dec. 2011.

[84] Y. R. Ramadan, H. Minn, and M. E. Abdelgelil, "Precompensation and system parameters estimation for low-cost nonlinear tera-hertz transmitters in the presence of I/Q imbalance," *IEEE Access*, vol. 6, pp. 51814–51833, 2018.

[85] M. A. Aygül, E. Memisoglu, and H. Arslan, "Joint estimation of multiple RF impairments using deep multi-task learning," in *Proc. IEEE Wireless Commun. Netw. Conf. (WCNC)*, Austin, TX, USA, Apr. 2022, pp. 2393–2398.

[86] N. Kolomvakis, M. Matthaiou, and M. Coldrey, "IQ imbalance in multiuser systems: Channel estimation and compensation," *IEEE Trans. Commun.*, vol. 64, no. 7, pp. 3039–3051, Jul. 2016.

[87] W. Zhang, R. C. De Lamare, and M. Chen, "Reduced-rank widely linear precoding in massive MIMO systems with I/Q imbalance," in *Proc. EUSIPCO*, Lisbon, Portugal, Sep. 2014, pp. 331–335.

[88] J. Tubbax, B. Come, L. Van der Perre, S. Donnay, M. Moonen, and H. De Man, "Compensation of transmitter IQ imbalance for OFDM systems," in *Proc. ICASSP*, Montreal, QC, Canada, Mar. 2004, pp. 325–328.

[89] Y. Li, C. Tao, G. Seco-Granados, A. Mezghani, A. L. Swindlehurst, and L. Liu, "Channel estimation and performance analysis of one-bit massive MIMO systems," *IEEE Trans. Signal Process.*, vol. 65, no. 15, pp. 4075–4089, Aug. 2017.

[90] S. Wang and L. Zhang, "Signal processing in massive MIMO with IQ imbalances and low-resolution ADCs," *IEEE Trans. Wireless Commun.*, vol. 15, no. 12, pp. 8298–8312, Dec. 2016.

[91] T. Liu, J. Tong, Q. Guo, J. Xi, Y. Yu, and Z. Xiao, "Energy efficiency of massive MIMO systems with low-resolution ADCs and successive interference cancellation," *IEEE Trans. Wireless Commun.*, vol. 18, no. 8, pp. 3987–4002, Aug. 2019.

[92] L. Fan, S. Jin, C.-K. Wen, and H. Zhang, "Uplink achievable rate for massive MIMO systems with low-resolution ADC," *IEEE Commun. Lett.*, vol. 19, no. 12, pp. 2186–2189, Dec. 2015.

[93] J. Jeong, S. H. Lim, Y. Song, and S.-W. Jeon, "Online learning for joint beam tracking and pattern optimization in massive MIMO system," in *Proc. IEEE Conf. Comput. Commun. (INFOCOM)*, Toronto, ON, Canada, Jul. 2020, pp. 764–773.

[94] Y. Song, J. Jeong, S. H. Lim, and S.-W. Jeon, "Joint beam tracking and pattern adaptation via online learning for massive MIMO systems," *IEEE Access*, to be published.

[95] H. V. H. Holma and P. Mogensen, "Extreme massive MIMO for macro cell capacity boost in 5G-advanced and 6G," Nokia, Espoo, Finland, White Paper CID210786, Oct. 2021.

[96] C. Han, J. M. Jornet, and I. Akyildiz, "Ultra-massive MIMO channel modeling for graphene-enabled terahertz-band communications," in *Proc. IEEE Veh. Technol. Conf. (VTC)*, Porto, Portugal, Jun. 2018, pp. 1–5.

[97] Y. Chen, L. Yan, C. Han, and M. Tao, "Millidegree-level direction-of-arrival estimation and tracking for terahertz ultra-massive MIMO systems," *IEEE Trans. Wireless Commun.*, vol. 21, no. 2, pp. 869–883, Feb. 2021.

[98] N. Shlezinger, G. C. Alexandropoulos, M. F. Imani, Y. C. Eldar, and D. R. Smith, "Dynamic metasurface antennas for 6G extreme massive MIMO communications," *IEEE Wireless Commun.*, vol. 28, no. 2, pp. 106–113, Apr. 2021.

[99] S. Tarboush, H. Sarieddeen, H. Chen, M. H. Loukil, H. Jemaa, M.-S. Alouini, and T. Y. Al-Naffouri, "TeraMIMO: A channel simulator for wideband ultra-massive MIMO terahertz communications," *IEEE Trans. Veh. Technol.*, vol. 70, no. 12, pp. 12325–12341, Dec. 2021.

[100] A. Liao, Z. Gao, D. Wang, H. Wang, H. Yin, D. W. K. Ng, and M.-S. Alouini, "Terahertz ultra-massive MIMO-based aeronautical communications in space-air-ground integrated networks," *IEEE J. Sel. Areas Commun.*, vol. 39, no. 6, pp. 1741–1767, Jun. 2021.
[101] J. Zhang, J. Zhang, E. Björnson, and B. Ai, "Local partial zero-forcing combining for cell-free massive MIMO systems," *IEEE Trans. Commun.*, vol. 69, no. 12, pp. 8459–8473, Dec. 2021.
[102] X. Guo, A. Camps, H. Park, H. Liu, C. Zhang, and J. Wu, "Phase and amplitude calibrations of rotating equispaced circular array for geostationary microwave interferometric radiometers—Theory and methods," *IEEE Trans. Geosci. Remote Sens.*, vol. 60, 2022, Art. no. 5300615.
[103] S. K. Yadav and N. V. George, "Coarray MUSIC-group delay: high-resolution source localization using non-uniform arrays," *IEEE Trans. Veh. Technol.*, vol. 70, no. 9, pp. 9597–9601, Sep. 2021.
[104] R. Zhang, W. Hao, G. Sun, and S. Yang, "Hybrid precoding design for wideband THz massive MIMO-OFDM systems with beam squint," *IEEE Syst. J.*, vol. 15, no. 3, pp. 3925–3928, Sep. 2021.
[105] Q. Wan, J. Fang, Z. Chen, and H. Li, "Hybrid precoding and combining for millimeter wave/sub-THz MIMO-OFDM systems with beam squint effects," *IEEE Trans. Veh. Technol.*, vol. 70, no. 8, pp. 8314–8319, Aug. 2021.
[106] C. Lin and G. Y. L. Li, "Terahertz communications: An array-of-subarrays solution," *IEEE Commun. Mag.*, vol. 54, no. 12, pp. 124–131, Dec. 2016.
[107] L. Yan, C. Han, and J. Yuan, "A dynamic array-of-subarrays architecture and hybrid precoding algorithms for terahertz wireless communications," *IEEE J. Sel. Areas Commun.*, vol. 38, no. 9, pp. 2041–2056, Sep. 2020.
[108] C. Han, L. Yan, and J. Yuan, "Hybrid beamforming for terahertz wireless communications: Challenges, architectures, and open problems," *IEEE Wireless Commun.*, vol. 28, no. 4, pp. 198–204, Aug. 2021.
[109] C. Lin, G. Y. Li, and L. Wang, "Subarray-based coordinated beamforming training for mmWave and sub-THz communications," *IEEE J. Sel. Areas Commun.*, vol. 35, no. 9, pp. 2115–2126, Sep. 2017.
[110] O. E. Ayach, S. Rajagopal, S. Abu-Surra, Z. Pi, and R. W. Heath, "Spatially sparse precoding in millimeter wave MIMO systems," *IEEE Trans. Wireless Commun.*, vol. 13, no. 3, pp. 1499–1513, Mar. 2014.
[111] H. Yuan, N. Yang, K. Yang, C. Han, and J. An, "Hybrid beamforming for terahertz multi-carrier systems over frequency selective fading," *IEEE Trans. Commun.*, vol. 68, no. 10, pp. 6186–6199, Oct. 2020.
[112] T. Mir, M. Waqas, U. Mir, S. M. Hussain, A. M. Elbir, and S. Tu, "Hybrid precoding design for two-way relay-assisted terahertz massive MIMO systems," *IEEE Access*, vol. 8, pp. 222660–222671, 2020.
[113] J. Tan and L. Dai, "THz precoding for 6G: Applications, challenges, solutions, and opportunities," 2020, *arXiv:2005.10752*.
[114] F. Gao, B. Wang, C. Xing, J. An, and G. Y. Li, "Wideband beamforming for hybrid massive MIMO terahertz communications," *IEEE J. Sel. Areas Commun.*, vol. 39, no. 6, pp. 1725–1740, Jun. 2021.
[115] A. M. Elbir, K. V. Mishra, and S. Chatzinotas, "Terahertz-band joint ultra-massive MIMO radar-communications: Model-based and model-free hybrid beamforming," *IEEE J. Sel. Topics Signal Process.*, vol. 15, no. 6, pp. 1468–1483, Nov. 2021.
[116] P. Wang, J. Fang, W. Zhang, and H. Li, "Fast beam training and alignment for IRS-assisted millimeter wave/terahertz systems," *IEEE Trans. Wireless Commun.*, vol. 21, no. 4, pp. 2710–2724, Apr. 2022.
[117] Q. Wu and R. Zhang, "Towards smart and reconfigurable environment: Intelligent reflecting surface aided wireless network," *IEEE Commun. Mag.*, vol. 58, no. 1, pp. 106–112, Jan. 2020.
[118] Z. Wan, Z. Gao, F. Gao, M. D. Renzo, and M.-S. Alouini, "Terahertz massive MIMO with holographic reconfigurable intelligent surfaces," *IEEE Trans. Commun.*, vol. 69, no. 7, pp. 4732–4750, Jul. 2021.
[119] K. Dovelos, S. D. Assimonis, H. Quoc Ngo, B. Bellalta, and M. Matthaiou, "Intelligent reflecting surfaces at terahertz bands: Channel modeling and analysis," in *Proc. IEEE Int. Conf. Commun. Workshops (ICC Workshops)*, Jun. 2021, pp. 1–6.
[120] Y. Yuan, Y. Zhao, B. Zong, and S. Parolari, "Potential key technologies for 6G mobile communications," *Sci. China Inf. Sci.*, vol. 63, no. 8, pp. 1–19, Aug. 2020.
[121] B. Ning, Z. Chen, W. Chen, Y. Du, and J. Fang, "Terahertz multi-user massive MIMO with intelligent reflecting surface: Beam training and hybrid beamforming," *IEEE Trans. Veh. Technol.*, vol. 70, no. 2, pp. 1376–1393, Feb. 2021.
[122] Q. Wu, S. Zhang, B. Zheng, C. You, and R. Zhang, "Intelligent reflecting surface-aided wireless communications: A tutorial," *IEEE Trans. Commun.*, vol. 69, no. 5, pp. 3313–3351, May 2021.
[123] W. Mei and R. Zhang, "Performance analysis and user association optimization for wireless network aided by multiple intelligent reflecting surfaces," *IEEE Trans. Commun.*, vol. 69, no. 9, pp. 6296–6312, Sep. 2021.
[124] Z. Li, H. Hu, J. Zhang, and J. Zhang, "RIS-assisted mmWave networks with random blockages: Fewer large RISs or more small RISs?" *IEEE Trans. Wireless Commun.*, vol. 22, no. 2, pp. 986–1000, Feb. 2023.
[125] Y. Pan, K. Wang, C. Pan, H. Zhu, and J. Wang, "Sum-rate maximization for intelligent reflecting surface assisted terahertz communications," *IEEE Trans. Veh. Technol.*, vol. 71, no. 3, pp. 3320–3325, Mar. 2022.
[126] N. Us Saqib, S. Hou, S. Ho Chae, and S.-W. Jeon, "Reconfigurable intelligent surface aided hybrid beamforming: Optimal placement and beamforming design," 2023, *arXiv:2303.11763*.
[127] N. U. Saqib, S. Hou, S. H. Chae, and S.-W. Jeon, "RIS-aided wireless indoor communication: Sum rate maximization via RIS placement optimization," in *Proc. IEEE Int. Conf. Commun. (ICC)*, Rome, Italy, May 2023.
[128] Z. Li, H. Hu, J. Zhang, and J. Zhang, "Coverage analysis of multiple transmissive RIS-aided outdoor-to-indoor mmWave networks," *IEEE Trans. Broadcast.*, vol. 68, no. 4, pp. 935–942, Dec. 2022.
[129] R. T. Alliance, "Reconfigurable intelligent surface technology," RIS TECH Alliance, China, White Paper, 2023, doi: 10.12142/RISTA.202302002.
[130] N. Abuzainab, M. Alrabeiah, A. Alkhateeb, and Y. E. Sagduyu, "Deep learning for THz drones with flying intelligent surfaces: Beam and handoff prediction," in *Proc. IEEE Int. Conf. Commun. Workshops (ICC Workshops)*, Jun. 2021, pp. 1–6.
[131] F. Sohrabi, T. Jiang, W. Cui, and W. Yu, "Active sensing for communications by learning," *IEEE J. Sel. Areas Commun.*, vol. 40, no. 6, pp. 1780–1794, Jun. 2022.
[132] Y. Lu, M. Hao, and R. Mackenzie, "Reconfigurable intelligent surface based hybrid precoding for THz communications," *Intell. Converged Netw.*, vol. 3, no. 1, pp. 103–118, Mar. 2022.
[133] Z. Zhang, T. Jiang, and W. Yu, "Learning based user scheduling in reconfigurable intelligent surface assisted multiuser downlink," *IEEE J. Sel. Topics Signal Process.*, vol. 16, no. 5, pp. 1026–1039, Aug. 2022.
[134] T. Jiang, H. V. Cheng, and W. Yu, "Learning to reflect and to beamform for intelligent reflecting surface with implicit channel estimation," *IEEE J. Sel. Areas Commun.*, vol. 39, no. 7, pp. 1931–1945, Jul. 2021.

NAJAM US SAQIB (Graduate Student Member, IEEE) received the B.S. and M.S. degrees in electronics engineering from COMSATS University Islamabad, Abbottabad, Pakistan, in 2010 and 2013, respectively. He is currently pursuing the Ph.D. degree with Hanyang University, Ansan, South Korea. He was a Lecturer with the Department of Electrical and Computer Engineering, COMSATS University Islamabad, from 2014 to 2019. His research interests include massive MIMO, hybrid beamforming, reconfigurable intelligent surfaces, and machine learning. He is an Active Member of IEEE and plans to continue his research work in academia to develop advanced wireless communication systems.

MUHAMMAD SAJID HAROON received the B.Sc. degree in electronics engineering from International Islamic University Islamabad, Pakistan, in 2007, the M.S. degree in electrical engineering from the COMSATS Institute of Information Technology, Attock, Pakistan, in 2013, and the Ph.D. degree from the Ghulam Ishaq Khan Institute of Engineering Sciences and Technology, Swabi, Pakistan, in 2020. He is currently a Postdoctoral Researcher with Hanyang University, ERICA Campus, Ansan, South Korea. His research interests include interference mitigation in cellular networks, 5G and 6G cellular networks, stochastic processes, aerial jammers, and metaheuristics algorithms.

HWI YOUNG LEE received the B.S. degree in semiconductor system engineering, in 2016, and the M.S. degree in electrical and computer engineering from Sungkyunkwan University, Suwon, South Korea, in 2018, where he is currently pursuing the Ph.D. degree with the Department of Electrical and Computer Engineering. He is also a Researcher with the Korea Testing Laboratory, Ansan, South Korea. His research interests include interference management, duplex evolution, beamforming, and artificial intelligence (AI)/machine learning (ML) in 5G-advanced air interfaces.

KWANGHYUN PARK received the B.S. and M.S. degrees in electrical and computer engineering from Sungkyunkwan University, Suwon, South Korea, in 2016 and 2018, respectively. Since 2020, he has been a Researcher with the Future Communication Technology Center, Korea Testing Laboratory, Ansan, South Korea. His research interests include interference management, duplex evolution, and MIMO enhancement in 5G and 5G-advanced mobile communication technologies.

HOON-GEUN SONG received the B.S. degree in electrical engineering from Hanyang University, Ansan, South Korea, in 1998, and the M.S. and Ph.D. degrees in communications and system from Hanyang University, Seoul, South Korea, in 2000 and 2019, respectively. In 2000, he joined LG Electronics, Anyang, Gyeonggi, South Korea, working in the area of the multipath searcher and the time tracker for the WCDMA UE modem development. In 2002, he was with Samsung Electronics, Suwon, South Korea, worked on the mobile communication research complex of the fourth generations mobile communications. He has been the Chief Engineer with the Korea Testing Laboratory, Ansan, since 2006. His research interest includes 5G and 5G-advanced mobile communication technologies.

SANG-WOON JEON (Senior Member, IEEE) received the B.S. and M.S. degrees in electrical engineering from Yonsei University, Seoul, South Korea, in 2003 and 2006, respectively, and the Ph.D. degree in electrical engineering from the Korea Advanced Institute of Science and Technology (KAIST), Daejeon, South Korea, in 2011. He is a Professor with the School of Computer Science and Technology, Zhejiang Normal University, Jinhua, China; and the Department of Electrical and Electronic Engineering, Hanyang University, Ansan, South Korea. From 2011 to 2013, he was a Postdoctoral Associate with the School of Computer and Communication Sciences, École Polytechnique Fédérale de Lausanne, Lausanne, Switzerland. His research interests include wireless communication, evolutionary computation, and machine learning.

He was a recipient of the Haedong Young Scholar Award, in 2017, which was sponsored by the Haedong Foundation and given by the Korea Institute of Communications and Information Science (KICS); the Best Paper Award of the IEEE International Conference on Communications, in 2015; and the Best Thesis Award from the Department of Electrical Engineering, KAIST, in 2012.